Dune erosion during storm surges

A review of the observations, physics and modelling of the collision regime

van Wiechen, P.P.J.; de Vries, S.; Reniers, A.J.H.M.; Aarninkhof, S.G.J.

DOI
10.1016/j.coastaleng.2023.104383

Publication date
2023

Document Version
Final published version

Published in
Coastal Engineering

Citation (APA)
van Wiechen, P. P. J., de Vries, S., Reniers, A. J. H. M., & Aarninkhof, S. G. J. (2023). Dune erosion during storm surges: A review of the observations, physics and modelling of the collision regime. *Coastal Engineering*, *186*, Article 104383. https://doi.org/10.1016/j.coastaleng.2023.104383

Coastal Engineering 186 (2023) 104383

Contents lists available at ScienceDirect

Coastal Engineering

journal homepage: www.elsevier.com/locate/coastaleng

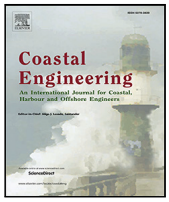

Review

Dune erosion during storm surges: A review of the observations, physics and modelling of the collision regime

P.P.J. van Wiechen *, S. de Vries, A.J.H.M. Reniers, S.G.J. Aarninkhof

Delft University of Technology, Mekelweg 5, 2628 CD Delft, Netherlands

ARTICLE INFO

Keywords:
Dune erosion
Storm surges
Collision regime
Review

ABSTRACT

Dune erosion during storm surges can lead to excessive damage to the dune system with devastating floods as a potential consequence. A risk assessment of areas protected by dunes can be facilitated by an understanding and description of the physical processes that take place. Field measurements, knowledge of underlying processes and numerical modelling have developed with time, which enabled a more comprehensive description and new predictive techniques. This review concerns dune erosion in the collision regime, and summarises relevant observations, describes underlying processes and explains existing models predicting dune erosion. Observations of dune erosion consist of field observations, laboratory experiments and manipulative field campaigns. The underlying physical processes that contribute to dune erosion are divided into processes that contribute to sediment transport due to hydrodynamic forcing, which occurs in the surf and swash zone, and sediment transport due to avalanching, which occurs in the swash zone, on the dune face and on the dune crest. The existing dune erosion models that are discussed here contain (empirical) equilibrium profile models and process-based models, which can both be a valuable tool for the risk assessment of storm surges. However, model uncertainties still remain, as specific processes are not yet fully understood and described. Examples are the influences of wave obliquity, sediment grain size, and vegetation on the dune face. By improving our knowledge through research and reducing these uncertainties, we can further improve our predictive models. This could eventually lead to more accurate predictions, more complete risk assessments, and sandy coastlines which are more resilient to excessive dune erosion and possible floods.

1. Introduction

Storm surges can lead to excessive dune erosion with devastating floods as a potential consequence. Barrier islands and low-lying countries protected by dunes are especially vulnerable to dune erosion. To assess the risks these areas face, an understanding and description of the physical processes that take place during dune erosion can be of value.

Storms can be classified into four regimes with different levels of impact (Sallenger, 2000). These regimes are the (1) swash regime, (2) collision regime, (3) overwash regime and (4) inundation regime. This review confines itself to dune erosion in the collision regime, when the total water level exceeds the dune foot causing waves to collide with the dune face and force erosion. The eroded sand is transported offshore where it settles in the outer surf (Fig. 1).

The induced damage to the dunes in the collision regime can be significant. On January 3 1976, a 1:20 year storm collided with the Dutch coast, resulting in dune retreat of 6–10 m along the Holland coast (Vellinga, 1978). In more recent times, Masselink et al. (2016b) reported erosion volumes of over 200 m^3/m along the beaches of Cornwall, UK, after the extreme storms during the winter of 2013/2014. Some of these beaches were completely stripped of sediment and exposed a rocky shore. Castelle et al. (2015) observed, for the same winter, a beach retreat of 20–30 m and average scarp heights of 6–8 m at erosion hotspots along the Gironde coast (France). Harley et al. (2016) analysed the 2007 and 2015 East Coast Lows at Narrabeen beach, Australia, and found average erosion volumes of 78 and 57 m^3/m, and a landward retreat of the subaerial beach of 28 and 19 m respectively.

This paper presents an overview of current knowledge on dune erosion in the collision regime. In the Section 2, field observations, laboratory experiments and *manipulative* field campaigns with regards to this topic are introduced. The Section 3 describes the relevant physical processes triggering erosion. The Section 4 summarises developed models to predict storm impact. In the Section 5 and final section, conclusions are drawn based on the information presented in this review.

* Corresponding author.
E-mail address: P.P.J.vanWiechen@tudelft.nl (P.P.J. van Wiechen).

https://doi.org/10.1016/j.coastaleng.2023.104383
Received 7 October 2022; Received in revised form 25 January 2023; Accepted 30 August 2023
Available online 2 September 2023

Fig. 1. Damage during the collision regime at the Holland Coast, the Netherlands (2022, Ph. Mischa Keijser).

2. Field and laboratory observations of dune erosion in the collision regime

2.1. Field observations

Field observations of dune erosion in the collision regime can date all the way to the 18th century (Baart et al., 2011). The observations can be a valuable tool for analysing dune erosion, as a coastal stretch is investigated under real-life conditions ensuring the inclusion of all relevant processes. Still, storm conditions prove dangerous for surveyors, making detailed temporal observations difficult and therefore limited. Researchers have often turned to pre- and post-storm surveys to determine morphologic change during the storm. The beach and dune morphology can be recorded using an RTK GPS (Seymour et al., 2005; Harley et al., 2016; Masselink et al., 2016a), LiDAR (both terrestrial and airborne) (Bonte and Levoy, 2015; de Winter et al., 2015; Overbeck et al., 2017), or photo imaging (Lippmann and Holman, 1990). The temporal characteristics of storm hydrodynamics have been recorded using different instruments, of which pressure sensors, velocimeters (both acoustic and electromagnetic), and wave buoys are used frequently (Reniers et al., 2004b; Seymour et al., 2005; Senechal et al., 2011; de Winter et al., 2015).

During storms, large hydrodynamic forcing changes the underwater profile, the beach and the dunes. Complex three-dimensional surf zone structures, indicating variability in alongshore direction, are usually destroyed, resulting in a linear uniform bar-trough system, after the classification of Wright and Short (1984) (Fig. 2) (Lippmann and Holman, 1990; Thornton et al., 1996; Stive and Reniers, 2003; Ranasinghe et al., 2004). This process is sometimes referred to as a morphological beach reset. Price and Ruessink (2011) stipulate the importance of the wave angle of incidence for this reset, as oblique waves trigger an alongshore current which can straighten alongshore bars. For example, Castelle et al. (2015) found that a normally incident high energy event increased alongshore variability by triggering megacusp formation due to the absence of alongshore currents.

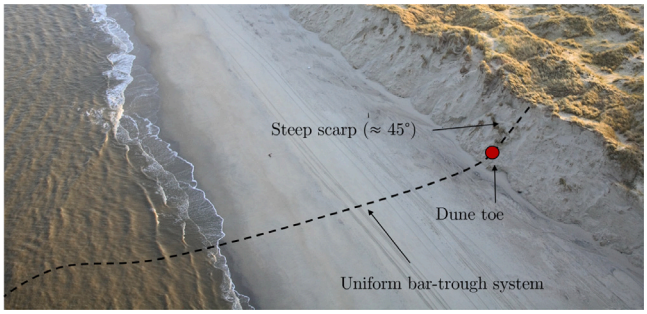

Fig. 2. Dune erosion at the coast of Vlieland, the Netherlands. Photograph by van Houdt (Dutch Ministry of Infrastructure and Water Management) (2008).

In cross-shore direction, the post-storm dune profile (Fig. 2) commonly shows a newly formed dune toe which can be related to the maximum water level or a certain wave runup level (Bonte and Levoy, 2015; van Bemmelen et al., 2020; de Winter et al., 2015). Above the dune toe, a scarp or steep slope can be observed, running upward to the top of the dune, under an angle of approximately 45° (Vellinga, 1978; Moller and Swart, 1988; Nishi et al., 1994; Splinter and Palmsten, 2012; de Winter et al., 2015). Below the dune toe, bed perturbations are suppressed and advected offshore during the storm, resulting in a smooth beach profile (Birkemeier et al., 1988; Steetzel, 1992; Stive and Reniers, 2003). Outer surf and offshore sand bars that were present before the storm usually migrate offshore during storm conditions (Gallagher et al., 1998).

2.2. Laboratory experiments

During the second half of the 20th and the beginning of the 21st century, numerous laboratory experiments were conducted to investigate dune erosion (see Table 1 for an overview). Within a confined laboratory environment where the hydrodynamic forcing could be controlled, it became possible to investigate the influence of specific hydrodynamic and morphodynamic parameters individually in time. The temporal evolution of the bed profile could also be recorded, which was less straightforward in field conditions. Moreover, due to the sheltered and controlled environment, more sophisticated measurement devices could be used, such as the stereo video imagery (Van Thiel De Vries et al., 2007; Palmsten and Holman, 2012).

Inside a wave flume, coastal profiles were built as a physical model. Scale factors were applied if the prototype sizes were too large for a laboratory. Small and large scale factors were applied to generate a laboratory setup capable of capturing dune erosion processes (van de Graaff, 1977; Hughes, 1981; van Gent et al., 2008; Palmsten and Holman, 2012). At the offshore boundary of the flume, a wave machine (e.g. wave piston or paddle) generated the hydrodynamic conditions. Vellinga (1986), Arcilla et al. (1994), and van Gent et al. (2008) performed tests in the Deltaflume of the Delft Hydraulics facility (Fig. 3). With an effective length of 225 m from the wave paddle, a width of 5 m and a depth of 7 m, its large dimensions accommodated horizontal spatial scale factors ranging from 1:5 to 1:1, of which the latter meant the prototype size was represented in the physical model.

Flume experiments were performed by van de Graaff (1977) and Vellinga (1981) to investigate the effect of the sediment grain size on the post-test dune profile. For beaches containing fine sediment with smaller settling velocities, which are associated with smaller grain sizes, they found larger total erosion volumes, a wider settling area, and a post-test profile with a milder beach slope and a lower dune toe. Later, Vellinga (1986) analysed the effect of different hydrodynamic parameters on the shape of the post-test profile. In both small and large scale flume experiments, he exposed the same dune to different hydrodynamic conditions. The post-test profiles showed similarities in shape, and he reasoned that a beach profile under storm conditions moves towards an equilibrium profile with respect to these storm conditions. Based on this reasoning and the results of the experiments, Vellinga developed the equilibrium model DUROS, which predicts the post-storm dune profile using the storm conditions and the properties of dune sediments. van Gent et al. (2008) later included the wave period in Vellinga's model, after large-scale flume tests revealed larger wave periods led to increasing dune erosion volumes. Moreover, van Gent et al. (2008) observed the presence of 2 stages in dune erosion. The initial stage consists of up-rush and backwash over the dune face and results in drag-induced erosion. This stage continues until the erosion

Table 1
Flume experiments reporting dune erosion. n_h is the depth scaling factor (if a specific prototype has to be represented within the setup), H_s is the significant wave height, T_p the peak period, SSL the storm surge level, and D_{50} the sediment diameter exceeded by 50% of the grains.

Location	n_h	H_s (m)	T_p (s)	SSL (m)	D_{50} (μm)	Reference
Delta Flume (NL)	– 6	1.4 0.5–1.5	5 4.90–7.35	4.6 4.5	220 200	Arcilla et al. (1994) Van Thiel De Vries et al. (2007) van Thiel de Vries et al. (2008) van Gent et al. (2008)
Oregon State University (USA)	6	1.3	4.9	0.17	230	Palmsten and Holman (2012)
Delft Hydraulics Laboratory (NL)	150, 84, 47, 26	0.05, 0.09, 0.16, 0.29	0.98, 1.31, 1.75, 2.35	0.03, 0.06, 0.11, 0.19	150–225	van de Graaff (1977)
University of Florida (USA)	25	0.07–0.12	0.97–1.357	0.10–0.17	152	Hughes (1981)
Delta Flume (NL)	5, 3.27, 1	1.5, 1.85, 2.00	5.4, 5, 7.6	4.2, 4.2, 5.00	150–225	Vellinga (1986)
Delft Hydraulics Laboratory (NL)	84, 47, 26	0.091, 0.163, 0.292	1.31, 1.76, 2.35	0.19, 0.11, 0.06	95, 130, 150, 225	Vellinga (1981)
						Vellinga (1986)
Delta Flume (NL)	–	1.4	5	4.6	220	Arcilla et al. (1994)
North Carolina State University (USA)	–	0.045–0.105	–	–	300	Overton et al. (1988)
North Carolina State University (USA)	–	0.045–0.141	–	–	220–780	Overton et al. (1994)
ACE Mississippi (USA)	10	0.06–0.20	2.2	0.53–0.58	130	Erikson et al. (2007)
Texas A&M University at Galveston (USA)	–	0.05	0.8	0.18	140	Figlus et al. (2014)
IIUNAM (Mexico)	–	0.10, 0.15	1.118, 1.5652, 2.012	0.50	142	Silva et al. (2016)
Texas A&M University (USA)	1	0.0431–0.0503	19.50	0.18	500	Feagin et al. (2019)

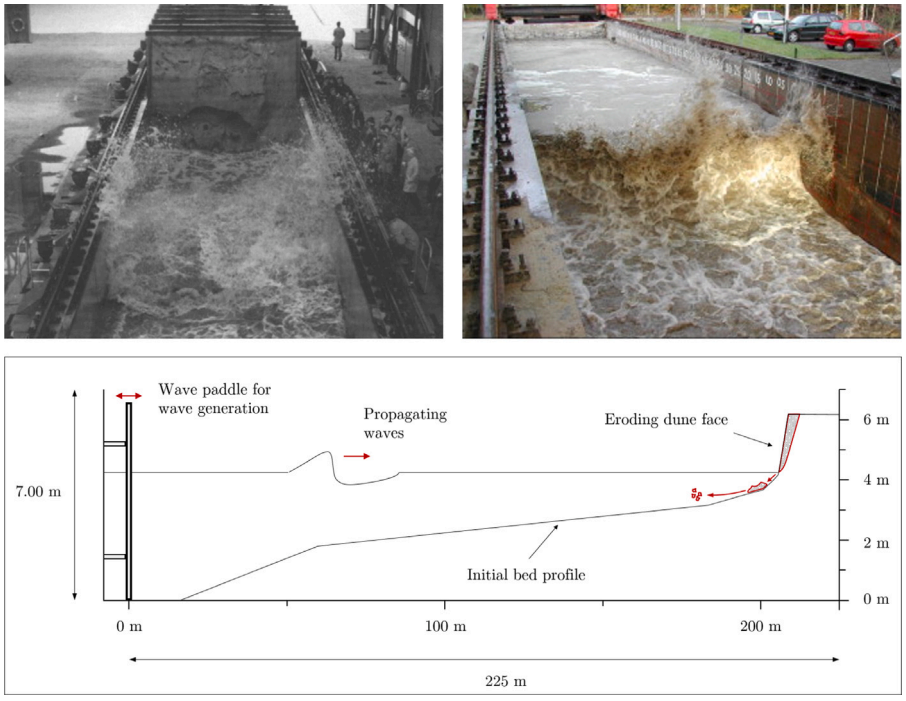

Fig. 3. Upper left: Large scale test in the Deltaflume performed by Vellinga (1982) (photograph from Vellinga (1986)). Upper right: Large scale test in the Deltaflume performed by van Gent et al. (2008) (photograph from same paper). Lower panel: schematisation of the Delta flume tests of van Gent et al. (2008).

causes the dune face to be nearly vertical or overhanging. At this point the second stage commences during which slumps of sediment fall down the dune face intermittently, a process referred to as avalanching.

This second stage in which avalanching occurs was studied intensively by Overton et al. (1994), Van Thiel De Vries et al. (2007), Erikson et al. (2007) and Palmsten and Holman (2012). The response

of the dune face to a single bore was studied using small-scale flume experiments by Overton et al. (1988). Each bore was generated by filling a head tank with water and releasing the water at once by raising the front gate. Eroded volumes from the dune were computed using photographs taken perpendicular on the wave flume, and could be correlated to the impact of the waves. Later, Overton et al. (1994) used a similar flume setup to study the effect of sediment grain size and dune compaction on dune face response. A dune was again exposed to one single bore, but this time the dunes were built with either a coarse sediment from North Carolina or a fine grain sand from Oregon. Within each sediment type, tests were performed with a dune with a high density or compaction, and a low density or compaction.

The types of soil failure leading to avalanching were studied in small-scale experiments by Erikson et al. (2007). An eroding dune was replicated using a vertical dune face and an equilibrium beach profile below it according to Dean (1977). In the experiments, dunes were subjected to waves until sufficient erosion occurred at the base of the dune to cause a slump to fall down.

The temporal variability and frequency of occurrence of avalanching was studied by Palmsten and Holman (2012) using stereo imagery. With images from 2 cameras, 3D reconstructions of an eroding dune were made before and after multiple wave impacts. In the experiments they observed that (1) dune erosion occurred only after water had infiltrated the dune for some time, (2) the slump usually involved only the wetted segment of the dune and (3) a stable state was reached when the dune toe eroded backwards and upwards, reducing the scarp height (Palmsten and Holman, 2011).

More recently, the effect of vegetation on avalanching has been investigated using flume experiments (Kobayashi et al., 2013; Figlus et al., 2014; Silva et al., 2016; Feagin et al., 2019). Kobayashi et al. (2013) used wooden dowels as an artificial representation of vegetation. Figlus et al. (2014), Silva et al. (2016) and Feagin et al. (2019) used actual vegetation in their flume experiments. The experiments showed that vegetation could both increase and decrease dune erosion volumes.

Still, laboratory experiments do not offer full closure to understanding all important processes during dune erosion. Natural conditions are not fully represented within laboratory experiments and there are chances that certain important natural processes are improperly replicated or overlooked. Especially, 2DH effects and associated alongshore variability cannot be included in flume experiments.

2.3. Manipulative field campaigns

The concept of *manipulative field campaigns* has been developed over the last decades to investigate dune erosion. In manipulative field campaigns, a field setup is built or altered in such a way that dune erosion is forced or very likely to occur under already moderate and therefore more frequent events. This increases the probability of acquiring field data on specific dune erosion processes. Other advantages are that (1) dangers and difficulties for observers in the field decrease because the conditions are less severe, (2) all natural processes, both cross-shore and alongshore, are included, and (3) the costs are usually lower than that of laboratory experiments.

Examples of manipulative field experiments are described in Fisher et al. (1986), Larson et al. (2004b), van Bemmelen et al. (2020), and Schweiger et al. (2020). Fisher et al. (1986) recreated a small dune in the swash zone to be attacked during high water, with the purpose of validating the linear relationship between the swash force and dune erosion volumes formulated in Fisher and Overton (1985). Larson et al. (2004b) changed the foreshore slope of 2 Pacific beaches in Japan with a bulldozer to see how and what sediment transport rates forced the beach back to its initial equilibrium. van Bemmelen et al. (2020) created several artificial mounds of sand in the intertidal zone, comparable to small-scale dunes, to investigate how beach scarps form and how the position of the dune toe changes during wave attack.

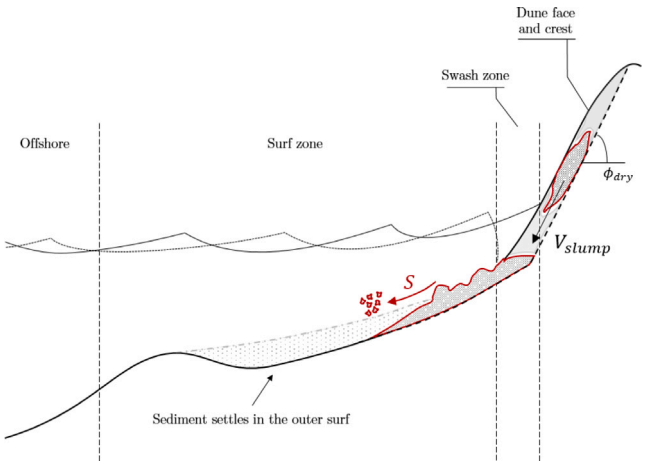

Fig. 4. Sediment transport due to hydrodynamic forcing occurs in the surf and swash zone (S, red arrow). Sediment transport due to avalanching occurs in the swash zone, on the dune face and on the dune crest (slumps with V_{slump} slide down the dune face, black arrow). Overall, sediment is eroded from the dunes and transported offshore towards the outer surf-zone.

Schweiger et al. (2020) created an artificial dune just above the high water line to evaluate how the model XBeach predicts dune erosion in the collision, overwash, and inundation regime after Sallenger (2000). The dune had an initial depression at its centre in alongshore direction, which forced inundation to occur there.

In general, manipulative field experiments provide the opportunity to investigate real-life conditions in a semi-controlled setting. In this semi-controlled setting, highly energetic conditions can be studied in detail while dangers for researchers are reduced.

In summary, field observations, laboratory experiments, and manipulative field experiments have given more and crucial insights in relevant hydrodynamic and morphodynamic processes occurring during dune erosion. These insights provided the basis for the development and validation of new theories and models, which form a valuable contribution towards a more comprehensive description of relevant processes and new predictive techniques.

3. Processes in dune erosion during storm surges in the collision regime

3.1. Types of sediment transport in dune erosion

Roughly two types of sediment transport can be distinguished: (1) transport due to hydrodynamic forcing and (2) transport due to avalanching of the dune face (Fig. 4). Sediment transport due to hydrodynamic forcing occurs in the surf and swash zone (Larson et al., 2004b; Masselink et al., 2005). Sediment transport due to avalanching is driven by soil instabilities and gravity, and occurs in the swash zone, on the dune face, and on the dune crest (Erikson et al., 2007; van Gent et al., 2008). Both will be elaborated upon separately in the sections below. Each section will first give a general description of the different mechanisms governing the type of transport, followed by an illustration of these mechanisms using run 2E of the LIP11D experiments described in Arcilla et al. (1994).

3.2. Sediment transport due to hydrodynamic forcing

3.2.1. General description

Waves and wave-induced currents erode sediment from the bed and transport it elsewhere. To describe the transport of sediment and the resulting bed level changes, many authors use the continuum approach, in which spatial differences in sediment transport are linked to bed

level changes in time (e.g. Steetzel (1993), Reniers et al. (2004a) and Roelvink et al. (2009)). Here, this approach will also be used to describe the important physical processes. In such a continuum approach, the horizontal transport of sediment at location (x, y) can be conceptualised and written as the product of the horizontal flow velocity and sediment concentration (Steetzel, 1993):

$$\vec{S}(x,y) = \int_{z=-d}^{\eta} c(x,y,z,t) \cdot \vec{u}(x,y,z,t) \mathrm{d}z \tag{1}$$

In this expression $\vec{S}$ is the time varying horizontal sediment transport rate integrated over depth, $\vec{u}$ is the time varying horizontal velocity vector at vertical location z, c is the time varying sediment concentration at vertical location z, d is the average water depth and η the time varying free surface elevation. During storm conditions, suspended sediment concentrations dominate over bed load (Ruessink et al., 1998), which means that vertical gradients in concentrations are limited.

Spatial gradients in the depth integrated sediment transport rates cause temporal changes in bed elevation (z_{bed}). In other words, when sediment transport rates increase (decrease) in the direction of flow, sediment has been picked up from (deposited on) the bed and erosion (deposition) must have occurred. This can be described using an Exner equation (e.g. Roelvink et al. (2009)),

$$\frac{\partial z_{bed}(x,y)}{\partial t} = \frac{1}{1-p}\left(-\frac{\partial \vec{S}(x,y)}{\partial x} - \frac{\partial \vec{S}(x,y)}{\partial y}\right) \tag{2}$$

with p being the porosity of the sediment. By quantifying velocities and sediment concentrations, sediment transport rates can in theory be computed using Eq. (1). The bed level changes can then be approximated using Eq. (2). However, the magnitude and amount of complexities involved in nearshore hydro- and morphodynamics makes this approximation very difficult. Therefore, some authors choose separating the hydrodynamic processes into different scales to account for the most significant processes and to average out small-scale complexities (Steetzel, 1993; Reniers et al., 2004a). A possible assumption is that high-frequency wave motion and turbulence are the stirring agent, and time-averaged and low-frequency wave motion are the transporting agent. Together, they drive the morphodynamics (Bowen and Doering, 1984; Vellinga, 1986; Steetzel, 1993; Smith and Mocke, 2002; Reniers et al., 2004a).

In this review, we separate the processes that govern sediment transport due to hydrodynamic action into processes on a wave-averaged, infragravity (IG), and intra-wave/micro timescale. This order was chosen because early formulations and process studies have focused on wave-averaged processes. Later, it was found that infragravity motions drive nearshore hydrodynamics. More recently, intra-wave and micro-timescale processes have been given more attention in process descriptions regarding dune erosion.

Wave-averaged timescale ($\gtrsim$300 s)

On a wave-averaged timescale, the vertical velocity structure in the surf zone is driven by wave breaking (Dyhr-Nielsen and Sørensen, 1970; Steetzel, 1993). In cross-shore direction, velocities are onshore directed in the upper section of the water column due to breaking-induced radiation stresses (Fig. 5). In the lower section of the water column, these onshore velocities are balanced by the offshore directed return current and undertow, which are strongest in the lower part of the water column and in regions where wave breaking is most intense (Stive and Wind, 1986; Reniers et al., 2004b). The fact that flow velocities are offshore directed in the lower part of the water column has implications for the transport of sediment, because here sediment concentrations are generally larger (Steetzel, 1993). In alongshore direction, oblique waves drive a wave-averaged current in the alongshore direction (Bowen, 1969; Longuet-Higgins, 1970). The alongshore current is greatest at the location of wave breaking. Here radiation stresses are largest and balanced by the bed shear stress induced by the alongshore current (Thornton and Guza, 1986). Tidal currents are often

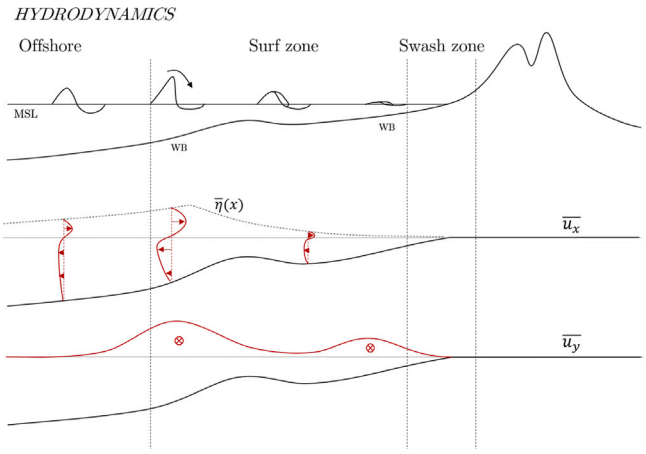

Fig. 5. Mean cross-shore ($\overline{u_x}$) and alongshore ($\overline{u_y}$) velocity profiles driven by wave action. WB stands for wave breaking.

categorised under the wave-averaged timescale because a tidal period is of larger order than the period of individual waves. The combination of all wave-averaged currents form an important driver for sediment transport.

Infragravity timescale (30 s $\lesssim T \lesssim$ 300 s)

On a timescale of approximately 30–300 s (after the classification of Munk (1950)), local hydrodynamics are dominated by infragravity waves (Fig. 6). These waves are generated by wave groups and when generated, bound to their wave group (Hasselmann, 1962; Longuet-Higgins and Stewart, 1962, 1964). They are released once the shorter waves of the group break, and when released, they can shoal, break and reflect on the beach as free waves (van Dongeren et al., 2007). Once reflected, they can remain in the surf zone (trapped or edge infragravity waves) or leave the surf zone and travel offshore, towards another coastal area (leaky infragravity waves, Herbers et al. (1995)). This means the incident infragravity wave field can contain both bound and free waves. A thorough review of infragravity waves is given in Bertin et al. (2018).

When wave conditions intensify to storm conditions, the increased contribution to nearshore hydrodynamics and dune erosion of infragravity waves is often dominant over that of short waves (Guza and Thornton, 1982; Bertin et al., 2018). This is because the intensification of offshore wave conditions leads to more energy within the low-frequency band, while the high-frequency band reaches saturation (Hughes et al., 2014; Fiedler et al., 2015). The increased infragravity energy leads to a stronger variation of the free surface and orbital velocities, a larger vertical range of the total runup levels, and more energetic infragravity bores on a timescale of ≈30–300 s. During periods of high water, in the crest of an infragravity wave, short wave energy and hydrodynamic action can reach further inland resulting in higher runup levels (Raubenheimer and Guza, 1996), and more wetting of the dune face. This wetting is important for avalanching (Palmsten and Holman, 2011). In the trough of an infragravity wave, the amount of depth-induced wave breaking increases, which increases the amount of sediment in suspension (Smith and Mocke, 2002). Depending on the time-varying net direction of flow at this location of intensified wave breaking, sediment transport can be either onshore or offshore (e.g. Osborne and Greenwood (1992), Smith and Mocke (2002) and Aagaard and Greenwood (2008)). In the swash zone, the backwash of infragravity waves themselves can attain considerable flow velocities, thereby exceeding a certain threshold for motion and stimulating offshore sediment transport (Osborne and Rooker, 1999).

Intra-wave and micro timescale ($\lesssim$30 s)

Processes occurring on the intra-wave and micro timescale contribute more to the concentration of suspended sediments (Smith and

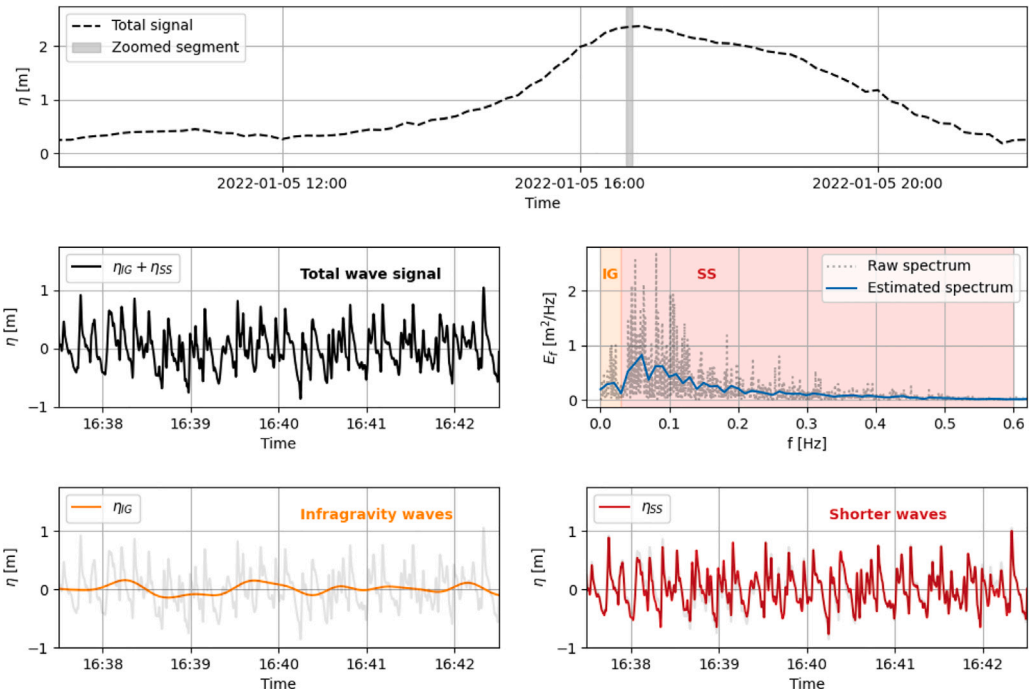

Fig. 6. Timeseries of a wave gauge deployed early 2022 at the Dutch coast near Kijkduin, the Netherlands. Through spectral analysis, the timeseries can be seperated into a wave-averaged signal (upper panel), infragravity signal (lower left) and intra-wave signal (lower right).

Mocke, 2002). van Thiel de Vries et al. (2008) performed qualitative experiments in the Deltaflume to investigate relevant processes that contribute to sediment concentrations. In the inner surf zone, which is dominated by wave breaking, the increased concentrations correlated well with the presence of steep, unstable wave fronts. Steep waves cause a larger pressure gradient, which results in a larger force exerted on the bed and increases sediment concentrations (Madsen, 1975; Masselink and Puleo, 2006). The instabilities at the wave front generate turbulence, which can reach the bed as a pulse and stir up sediment (Dally and Dean, 1984; Roelvink and Stive, 1989; Butt et al., 2004). Because longer waves can attain a larger wave steepness, longer waves are more efficient in stirring up sediment, leading to increased dune erosion volumes (van Thiel de Vries et al., 2008). The increased concentrations in the surf zone measured by van Thiel de Vries et al. (2008) correlated less well with the measured near-bed flows and the associated bed shearing, contradicting earlier measurements such as van Rijn (1984) and Nielsen (1992).

Sediment concentrations are up to one order of magnitude larger in the swash zone when compared to the surf zone (Osborne and Rooker, 1999; Butt and Russell, 1999; Masselink et al., 2005). Puleo et al. (2000) analysed suspended sediment concentrations at three cross-shore locations in the swash zone using velocity, sea surface, and sediment concentration measurements. Significant differences in underlying processes are present between the uprush and backwash in the swash zone. During uprush, bore-generated turbulence (turbulent kinetic energy) strongly and directly influenced local suspended sediment concentrations. The suspension was high and nearly vertically uniform above the lower 1–2 cm of the water column. Just before flow reversal, the sediments settled rapidly. After flow reversal, backwash sediment concentrations increased with flow duration, but this time the distribution was less uniform with highest concentrations in the region very near to bed, with strong gradients going upward.

The effectiveness of the processes above to stir up and transport sediment depends on the shape (Cohn et al., 2019) and morphologic characteristics of the beach and dune system, including sediment grain size and dune compaction or density (Davidson et al., 2020). Vellinga (1981) found experimentally that smaller grain sizes yield larger dune erosion volumes, a wider area of sediment deposition with a milder slope (in cross-shore direction), and a higher post-storm dune toe. Vellinga's findings were confirmed numerically by Kriebel and Dean (1985).

3.2.2. Illustrations of the described hydrodynamic processes using run 2E of the LIP11D experiments

In 1993, the LIP11D experiments were carried out in the Delta Flume, the Netherlands, to identify the important physical processes in dune erosion (Arcilla et al., 1994). In test 2E, a dune with a crest just below 6 m was subjected to an 18 h storm with a surge level (SSL) of 4.6 m, a significant wave height H_s of 1.4 m and a peak period T_p of 5 s (Table 1). Among the deployed instruments was a measurement carriage equipped with, among other instruments, 5 velocimeters and 10 suction tubes which sampled sediment concentrations once each hour. During the storm simulation, wave conditions were run for one hour and then paused to record bed profiles using a bed profiler and shift the carriage to a new cross-shore position. Fig. 7 displays the vertical mean cross-shore velocity profiles and the sediment concentrations recorded by the suction tubes at several cross-shore positions, and the bottom profile at the beginning of the experiment and after 8 h of wave conditions.

Wave breaking commences at the bar at approximately x = 130 m (Fig. 7, upper panel), resulting in a larger offshore-directed wave-averaged undertow near the bed at locations x = 145 m, 152 m, and 160 m. This increase does not necessarily result in larger sediment concentrations, as location x = 160 m displays considerably higher concentrations for similar flow velocities. These higher concentrations are consistent with the notion that sediment concentrations in the swash zone are one order of magnitude larger than in the surf zone (Osborne and Rooker, 1999; Butt and Russell, 1999; Masselink et al., 2005).

3.3. Sediment transport due to avalanching

3.3.1. General description

On the dune face, on the dune crest, and partially in the swash zone, dune erosion is driven by sediment transport due to avalanching.

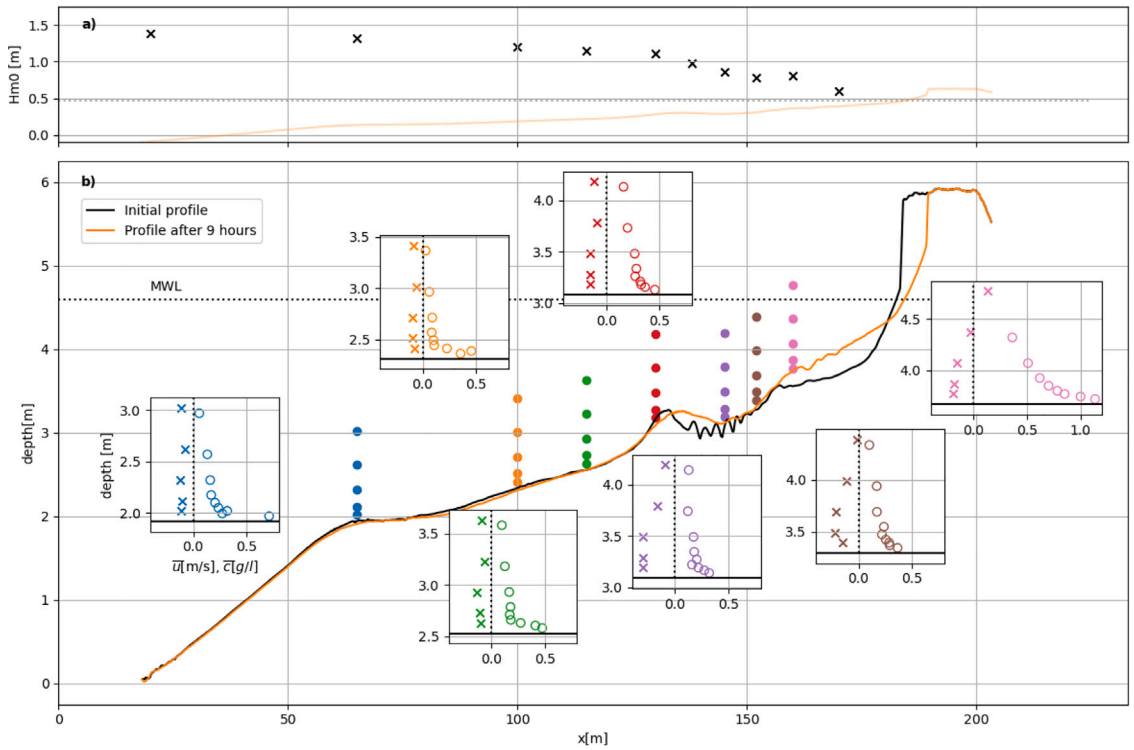

Fig. 7. LIP11D experiment 2E. (a) Significant wave height along flume based on pressure sensors. (b) Profile change after 8 h of storm conditions, and during 1 h wave-averaged flow velocities (crosses), $\overline{u}$, and sediment concentrations (open circles), $\overline{c}$, along 7 cross-shore transects based on carriage measurements. The measurement locations of the velocities are denoted with filled circles. The black dotted line represents the mean water level (MWL).

Avalanching is initiated by soil instabilities, and is a recurring process in which slumps of sediment slide down the dune face repeatedly due to gravity (van Thiel de Vries et al., 2008). These slumps provide a source of sediment for the transport driven by hydrodynamic action in the swash and surf zone (Fig. 8).

The instabilities are caused by the waves colliding with the dune face. These waves erode the lower part of the dune face through drag induced sediment transport, gradually steepening the dune face. The steepening can be accompanied by the formation of a notch at the dune toe (Erikson et al., 2007). At the same time, water infiltrates the front horizontally due to capillary action, and this infiltration increases the apparent cohesion of the wetted sediments (Palmsten and Holman, 2011). This apparent cohesion can cause a dune face with a slope well exceeding the angle of repose of dry sand (≈45°, e.g. Nishi et al. (1994)). The steepening can continue until the dune face is nearly vertical or overhanging. This, together with a potential notch, leads to a very unstable dune face which will eventually fail. The failure mechanism can either be of the shear-type or beam-type. With shear-type failure the weight of the overhanging layer of sediment becomes too large causing a block of sediment to fall down. With beam-type failure, a tensile crack forms more landward of the unstable front and a portion of the dune slides down. Erikson et al. (2007) observed beam-type failure more frequently than shear-type failure in their experiments.

The volume of the slumps have been related to the degree of horizontal infiltration (Palmsten and Holman, 2011). The apparent cohesion keeps the wetted sediment together and causes it to slump as a single unit. Given that the dry area of a dune is not influenced by apparent cohesion, the sediment above the wetted slump slides down along the angle of repose (W_2 along ϕ_{dry} in Fig. 8). This would imply that higher dunes reach larger erosion rates, as the dry volume is larger and the source of sediment to the swash zone increases. That higher dunes erode faster than lower dunes was confirmed in numerical studies by van Thiel de Vries et al. (2011) and Itzkin et al. (2021), and field observations by de Winter et al. (2015). In addition, they find larger erosion rates for steeper dunes, which could be attributed to the dune face becoming unstable faster because its initial slope is already quite steep.

The slumps that slide down the dune face temporarily defend the dune face from wave impact. The incident waves gradually transport the sediment of the fallen slump offshore until the dune face is exposed again. At this point the cycle as depicted in Fig. 8 restarts. With time, a new coastal profile develops with the sediment that slid down the dune face. This new profile decreases the amount of waves reaching the dune face, thereby decreasing in time the amount of sediment transported due to soil instabilities (Van Thiel De Vries et al., 2007).

Overton et al. (1994) studied the effect of sediment grain size and compaction on the volume of an individual avalanching event. A smaller grain size results in a larger capillary rise or a higher negative pore pressure within the dune, requiring a larger force to be eroded. With this reasoning, a smaller sediment grain size and larger compaction would result in smaller slumps. They confirmed these hypotheses in flume tests, in which the eroded volume of a vertical dune face after 1 single bore was analysed for dunes with different grain size and density, but identical foreslope.

The presence of vegetation on the dune face is important to consider when regarding sediment transport due to avalanching. However, the net effect of vegetation on dune erosion remains difficult to quantify due to the hydrodynamic, morphodynamic, and biologic complexities involved (Figlus et al., 2022). Multiple flume studies with real vegetation find smaller erosion rates and quantities for dunes covered with

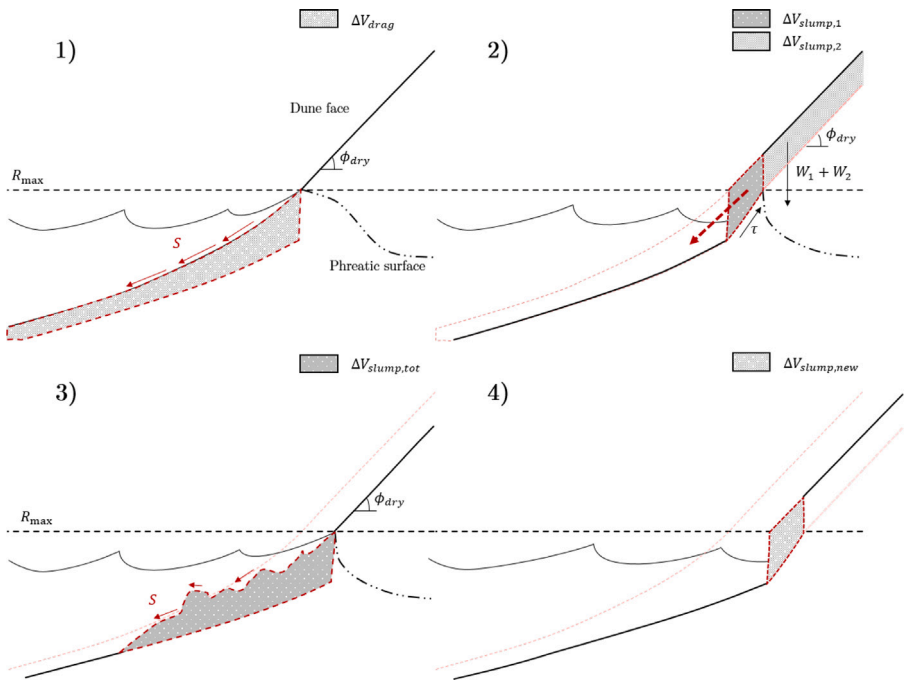

Fig. 8. Sediment transport due to soil instabilities displayed as a continuous cycle. (1) drag-induced erosion (S) removes sediment below the maximal runup level (R_{max}), steepening the dune face up to angles exceeding the natural angle of repose of dry sand (ϕ_{dry}). (2) incoming swash collides with the dune scarp, wetting dune sediments. At a certain moment, the weight of the wetted sediments (below the phreatic surface) and the dry layers above ($W_1 + W_2$) exceeds the resisting shear forces (τ), resulting in a slump falling down (red arrow). (3) After collapse, the sediment from the fallen slump is brought in suspension and transported offshore (S). (4) The cycle restarts.

vegetation (Silva et al., 2016; Feagin et al., 2019; Mendoza et al., 2017; Odériz et al., 2020; Figlus et al., 2022).

During the initial stages of a storm, in which waves run up and down the foreshore and dune face, vegetation above the bed primarily reduce erosion by attenuating swash and run-up bores (Barbier et al., 2008; Feagin et al., 2019). The vegetation below the bed decreases erosion by increasing the cohesion of sediments, which increases the resistance of the dune (Figlus et al., 2014; Davidson et al., 2020), but it can also partially increase erosion through a process called uprooting: when vegetation is pulled out of the bed through hydrodynamic action their roots can take large portions of sediment with them. Once the vegetation is pulled out, the roots attenuate waves and reduce erosion (Feagin et al., 2019). Figlus et al. (2014) finds that the below-ground effects are more significant due to the relatively short extent of the above-ground vegetation in the cross-shore. During later stages of a storm and avalanching, dune vegetation and their roots can slow down dune retreat Figlus et al. (2014). This reduction was found to increase with an increase in vegetation maturity, which also enhanced resistance to vertical shearing.

3.3.2. Illustrations of the described hydrodynamic processes using run 2E of the LIP11D experiments

The processes discussed above can again be identified in run 2E of the LIP11D experiments, described by Arcilla et al. (1994). Fig. 9 displays the development in time of the foreslope, dune toe, and dune face due to the storm conditions described in Section 3.2.2. The upper panel displays profile development in time, and marks the location of the dune toe, which is defined as the location where the second derivative of the bed profile is maximal. The derivatives of the bed profile are computed using second order accurate central differences, after applying a moving average of 20 cm on this profile to remove noise. The lower panel of Fig. 9 displays the angle of the bed at each cross-shore location, computed using the tangent with central differences.

The amount of erosion and retreat of the dune crest decreases with time, in accordance with the findings of Van Thiel De Vries et al. (2007) and Palmsten and Holman (2011). The dune toe retreats backwards and upwards in time, but seems to converge to a vertical elevation of approximately 5.25 m after 6 h and remains at that vertical elevation more or less. Only at t = 12 h the dune toe seems higher, possibly due to a slump event just before t = 12 h, which is supported by the less distinct transition from foreslope to dune face in the profile at that time. Above the dune toe, the angle of the dune face appears to remain constant at 61°. The vertical level of 5.25 m to which the dune toe converges can be linked to the maximal water level because (1) once this elevation is reached, the sediment above the toe remains dry, confirmed by the constant angle of the dune face of 61°, and (2) according to Palmsten and Holman (2011) the infiltration decreases with time and with that the erosion decreases. This means the profile should converge to a profile in which the infiltration at the dune face approaches zero, which occurs when the dune base is at the height of the maximal water level.

3.4. 2DH processes and variability in dune erosion

Up until the late 20th century, dune erosion was widely studied as a cross shore (1-dimensional or 2-dimensional vertical) mechanism (Vellinga, 1986). This gradually changed in the beginning of the 21st century. The horizontal alongshore dimension was included more often after numerical and field studies pointed out its importance in the hydrodynamics and morphodynamics during dune erosion (Thornton et al., 2007; Den Heijer, 2013; de Winter et al., 2015).

Important hydrodynamic processes acting on a 2DH scale are the directional spreading of waves and wave obliquity. The directional spreading of waves has an impact on the transfer of energy from the incident short wave band to the infragravity band. Waves with a larger difference in incident wave angle lead to smaller wave-wave interactions, and thus, less energy in the infragravity band (Herbers et al., 1994).

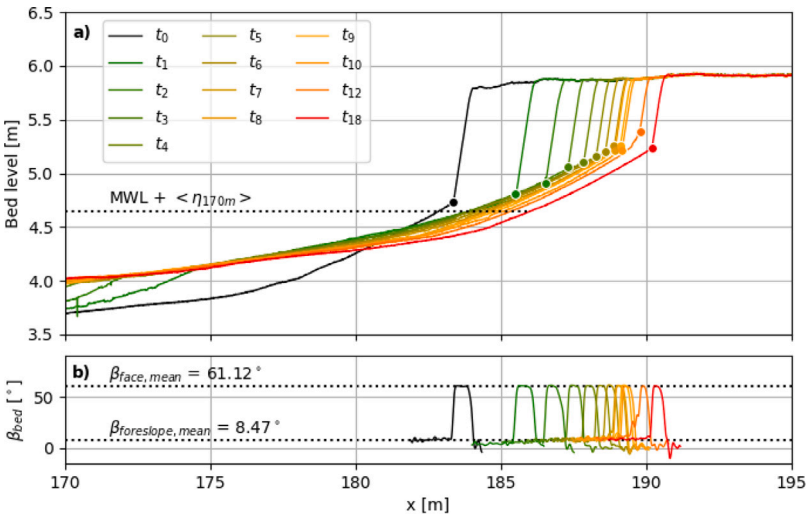

Fig. 9. Development of the foreslope, dune toe, and dune face in time for run 2E of the LIP11D experiments (Arcilla et al., 1994). Panel (a) displays profile development in time, and marks the location of the dune toe. The dotted line represents the mean water level (MWL) and the wave setup η at x = 170 m. Panel (b) displays the angle of the bed before the dune and dune face for each of the profiles. The dotted lines represent the mean of both angles.

The effect of wave obliquity acts both on the infragravity timescale, and the intra-wave and micro timescale. Oblique infragravity waves can get trapped in the nearshore (Herbers et al., 1995). After oblique infragravity waves reflect of the coastline, depth-induced refraction can cause the waves to turn back towards the coast. As a consequence, energy within the infragravity band can remain trapped in the surf zone affecting nearshore hydrodynamics.

On the intra-wave and micro timescale, oblique wind and swell waves have an effect on both the nearshore hydrodynamics and morphodynamics, and thus on nearshore sediment transport. However, their net effect on dune erosion is, to the author's knowledge, not yet fully understood. On one hand the cross-shore energy is smaller for oblique waves compared to shore-normal waves, reducing the maximal runup and magnitude of the undertow. On the other hand, oblique waves drive an alongshore current and this alongshore current might enhance sediment concentrations due to bed shearing. Because both the velocity and concentration profiles determine the magnitude of the sediment transport (see Eq. (1)), the net effect of oblique waves is not yet fully understood and requires further research, as it can potentially enhance dune erosion.

Alongshore variability in morphology of the sub- inter- and supratidal zones can also lead to alongshore variability in erosion rates. In the sub- and intertidal zone, differences in bathymetry influence both the velocity and concentration profiles, which in turn influence the gradients of sediment transport and thus erosion patterns (Eqs. (1) and (2)). This can lead to local 'erosion hotspots', locations along the shoreline with considerable more erosion and thus a greater risk of flooding (Castelle et al., 2015; Cohn et al., 2021). Variability in dune height, location, and steepness in the supratidal zone can lead to alongshore differences in sediment transport due to soil instabilities. van Thiel de Vries et al. (2011) argues that higher dunes lead to larger erosion volumes, because more sand will slump onto the beach. de Winter et al. (2015) ascribes variability in erosion of the upper profile to differences in dune face steepness and the presence of embryo dunes in front of the main dune.

Altogether, these findings suggest that dune erosion cannot always be regarded as a 1-dimensional mechanism. For specific wave conditions and beaches, a 2D evaluation of the nearshore hydrodynamics, morphodynamics, and morphology might be necessary. Because the net effect and relative importance of several 2DH processes is not yet fully understood, more research into these processes is recommended.

4. Modelling dune erosion in the collision regime

The increased knowledge on underlying hydrodynamic and morphodynamic processes have facilitated the development of dune erosion models. These models can be valuable tools when assessing the vulnerability of dune systems to storm surges. Dune erosion models can be roughly distinguished into 2 types: equilibrium models and process-based models. These models differ in the underlying physical basis, the degree of complexity, and the range of suitable hydrodynamic conditions and coastlines they can be applied to.

4.1. Equilibrium models

Equilibrium models estimate the post-storm cross-shore profile which develops when exposed to constant storm conditions for a sufficiently long time. This profile is assumed to be in short-term equilibrium with the storm conditions. This approach is based on the time-dependent negative feedback mechanism between the hydrodynamics and the morphodynamics: waves erode sediment from the dunes and transport it to the surf zone where it settles, forming a more dissipative coastal profile. As a consequence the wave impact on the dune is reduced with time, and this gradual reduction leads to a steady-state or equilibrium profile, where the net cross-shore sediment transport is approximately zero.

Equilibrium models have often been developed using laboratory experiments in which a dune is subjected to a storm for a prolonged period (Schijf, 1972; Vellinga, 1986; van Gent et al., 2008). Some equilibrium models first establish the shape of the empirically derived post-storm profile, and then fit this profile by shifting it shoreward until the eroded volume equals the settled volume so that sediment conservation is preserved (Fig. 10).

Modelling the short-term equilibrium response of dunes to storms was first attempted by Edelman (1972), who based his approach on the long-term equilibrium theory of Bruun (1954). Edelman observed that the upper post-storm profile below the storm surge level was almost always identical after storm surges, and attempted to estimate dune retreat using a volume balance such as the one displayed in Fig. 10. Later, van de Graaff (1977) found that the cross-shore length of post-storm profiles was less than that of Edelman's profiles, and that it did not extend beyond the surf zone. This meant that less sediment was required for the equilibrium profile, which leads to a less shoreline retreat in model predictions.

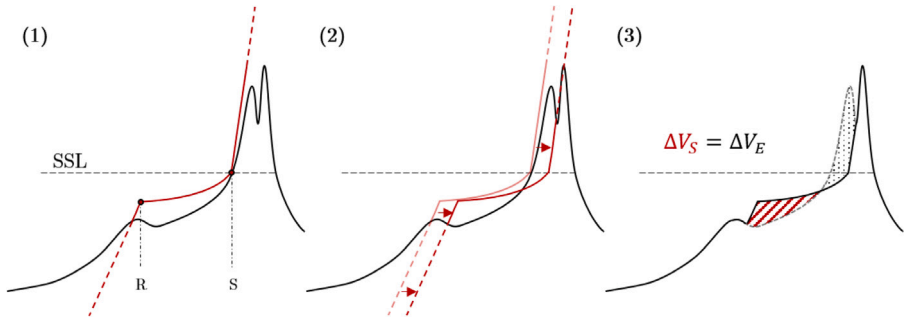

Fig. 10. General application of equilibrium profile models. First (1), the post-storm equilibrium profile is drawn (red) for a given cross-shore bathymetry (black). Next (2), the post-storm profile is shifted in shoreward direction until the eroded volume equals the settled volume and sediment conservation is preserved (3).

Vellinga (1986) proceeded with Edelman's and van de Graaff's approach and studied post-storm equilibrium profiles through large-scale laboratory tests to predict the amount of dune erosion during storms (Table 1). This resulted in the equilibrium model DUROS, which predicts a post-storm equilibrium profile that depends on the increased surge level, the offshore significant wave height, and the sediment fall velocity. The post-storm equilibrium profile can be built out of 3 sections, which can be separated by 2 transition points (R and S, Fig. 10). In offshore direction, the first transition point S is the newly formed dune toe, which is vertically fixed at the maximal storm surge level (SSL). Onshore of this point, the profile runs upward towards the dune berm with a 1:1 slope. Offshore of this point, the profile has a parabolic shape. This parabolic shape is described by

$$\frac{7.6}{H_{0s}} \cdot y = 0.47 \left[\left(\frac{7.6}{H_{0s}} \right)^{1.28} \cdot \left(\frac{w_s}{0.0268} \right)^{0.56} \cdot x + 18 \right]^{0.5} - 2.0 \tag{3}$$

where y is the vertical coordinate with respect to the storm surge level, $H_{0,s}$ is the offshore significant wave height, w_s the sediment fall velocity, and x is the cross-shore distance with respect to the first transition point S. The parabolic profile continues in offshore direction up to the second transition point R with coordinates:

$$x_R = 250 \cdot \left(\frac{H_{0s}}{7.6} \right)^{1.28} \cdot \left(\frac{0.0268}{w_s} \right)^{0.56} \tag{4}$$

$$y_R = 5.717 \cdot \left(\frac{H_{0s}}{7.6} \right) \tag{5}$$

Further offshore of the second transition point, the profile follows a 1:12.5 slope to the bed. The final profile location can be found iteratively by shifting the entire profile in onshore direction until all sediment is conserved (Fig. 10). To derive the coefficients in Eq. (3), Vellinga (1986) performed experiments with the normative storm conditions that are representative for the Dutch coast, with prototype values of H_0 = 7.6 m, T_p = 12 s, w_s = 0.0268 m/s, and a storm surge level of 5 m. These storm conditions are clearly reference values in the equations.

Fig. 11 displays model results of a storm hitting the coast of Meijendel, the Netherlands. The bed profile is retrieved from the open-source JARKUS dataset, provided by the Dutch Ministry of Infrastructure and Water Management (transect 8009600 of 2021). The storm conditions are based on the Dutch design conditions for this specific transect, and consist of a surge level of 5.44 m, a significant wave height of 8.26 m, a peak period of 13.80 s, and normally incident waves on a barred beach with sediment with a fall velocity of 0.0268 m/s.

Later, a term to account for the spectral mean wave period, $T_{m-1,0}$, was included in the DUROS model after large-scale flume experiments revealed that a larger spectral mean wave period led to more dune erosion (van Gent et al., 2008). The new version of the model was named DUROS+, and the spectral mean wave period was included in the formulation of the parabolic segment of the profile and the y-coordinate of the second transition point R:

$$\frac{7.6}{H_{0s}} \cdot y = 0.4714 \cdot \left[\left(\frac{7.6}{H_{0s}} \right)^{1.28} \cdot \left(\frac{10.9}{T_{m-1.0}} \right)^{0.45} \cdot \left(\frac{w_s}{0.0268} \right)^{0.56} \cdot x + 18 \right]^{0.5} - 2.0 \tag{6}$$

$$y_R = \left(\frac{H_{0s}}{7.6} \right) \cdot \left[0.4714 \cdot \left(250 \cdot \left(\frac{10.9}{T_{m-1.0}} \right)^{0.45} + 18 \right)^{0.5} - 2 \right] \tag{7}$$

The x-coordinate of the second transition point R remains unaltered. The minimal value for the wave period in Eqs. (6) and (7) is 10.9 s. This means that for storms with a smaller characteristic wave period, a $T_{m-1,0}$ of 10.9 s should be used nonetheless. Model results are displayed

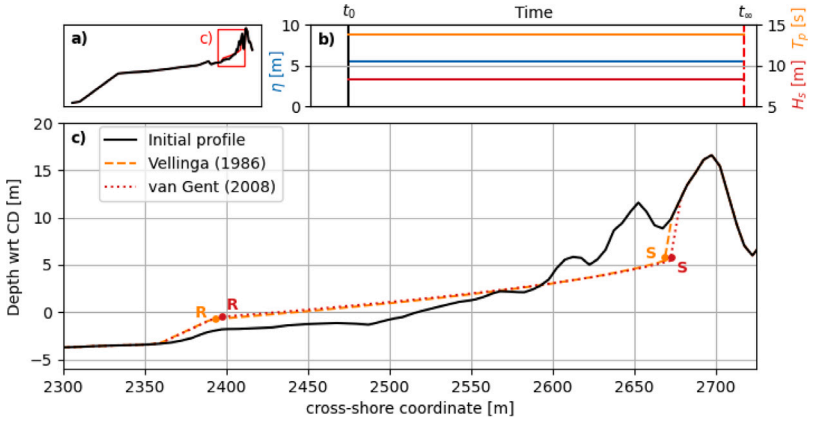

Fig. 11. Post-storm profiles (c) with respect to a given chart datum (CD) according to Vellinga (1986) (yellow) and van Gent et al. (2008) (red) for design storm conditions (b) on the Meijendel transect (c).

in Fig. 11, where it can be seen that DUROS+ predicts slightly larger erosion volumes due to the inclusion of the peak period of 13.80 s. To date, DUROS+ is used for the national safety assessment of the 250 km of dunes in the Netherlands.

Advantages of equilibrium models are that they are very easy to apply, computationally cheap, and in some cases validated through laboratory experiments. Disadvantages are that (1) equilibrium theory assumes the storm to be of sufficient duration for the equilibrium to be reached, which is not always the case, (2) hydrodynamic conditions change during a storm, meaning the equilibrium profile changes with time as well, (3) the models are calibrated on current representative hydrodynamic and morphodynamic data, making them less reliable for wave conditions that deviate strongly from these representative values.

Semi-equilibrium models provide a possible solution for insufficiently long storms or storms with temporal variability (Kriebel and Dean, 1985; Kobayashi, 1987; Larson and Kraus, 1989). Kriebel and Dean (1985) and Larson and Kraus (1989) presume the existence of an equilibrium dissipation rate D_{eq}, and base local sediment transport rates $S_{x,y}$ on the deviation of the actual dissipation rate D in time with this equilibrium dissipation rate D_{eq}. The change in bed level with time is then computed using the 1-dimensional Exner equation (Eq. (2) without the y-dimension). Avalanching is incorporated in the model of Larson and Kraus, called SBEACH, by redistributing sediment into neighbouring cells once the angle of repose of the sediment is exceeded.

Nevertheless, (semi-) equilibrium models can be difficult to apply to more complex coastal stretches. Examples of complexities are different sediment layers, vegetated dunes, and non-erodible structures such as revetments and seawalls. Also 2DH variabilities in hydrodynamics and bathymetry are difficult to include. Meanwhile, these complexities are found frequently along sandy coasts. For these coasts a different modelling approach, such as process-based modelling, might provide a solution.

4.2. Process-based models

Process-based models simulate the hydrodynamic and morphodynamic processes that occur during dune erosion. Changes in bed profiles are computed in both space and time. The underlying physical processes are represented in a given model domain by analytical expressions, which are solved numerically. The model domain can be separated into multiple cells, allowing specific characteristics to be assigned to each cell. This increases the amount of computational effort, the complexity of the model, and the amount of user-defined input to solve these processes, but allows inclusion of complexities such as revetments, non-erodible structures and vegetation. Process-based models often use a morphodynamic feedback loop for each timestep: (1) solve hydrodynamic processes in a given bathymetry at t_n, (2) use the hydrodynamics to compute sediment transport and bed level changes, (3) update the given bathymetry with the computed bed level changes, and (4) restart the loop: compute hydrodynamics for the new bathymetry at t_{n+1}. In this review we highlight different process-based models which are based on different theories and underlying assumptions. Where applicable we use model results that are original to this review to illustrate implications of important assumptions.

The 1-dimensional cross-shore process-based DurosTA model, developed by Steetzel (1993), bases bathymetry changes on gradients of sediment transport rates. The sediment transport rates are defined as the vertically integrated product of the mean flow and mean concentration (comparable to Eqs. (1) and (2)). The mean flow is defined by the local hydrodynamic conditions, which depend on the local wave height computed using a wave height decay model. The mean concentration profile is based on a reference bed concentration, calculated using the wave energy balance, and a vertical distribution function of the concentration, based on a vertical, non-stationary diffusion equation. Avalanching is not included in the model. Instead, bed erosion of the last wet cell is redistributed over this cell and the two shoreward adjacent dry cells, resulting in dune crest retreat. The negative feedback mechanism between the hydrodynamics and morphodynamics is included by computing the new bathymetry after each timestep, and using this updated bathymetry to compute the hydrodynamics for the next timestep. DurosTA allows boundary conditions to vary with time, which means a storm hydrograph with varying water level, wave height and wave period can be set as model input. Fig. 12 displays model results for the same coastal profile as Fig. 11, exposed to a storm as described by the storm hydrograph in Fig. 12b. The total computed storm duration is 32 h, with 3 high tides based on an M2 tide.

Steetzel (1993) specifically addresses the effect of high revetments, low revetments, and nearshore low dams as non-erodible structures within the coastal profile. DurosTA predicts the development of a pronounced scour hole at the toe of such a structure, which is in agreement with laboratory observations. However, the final scour depth is generally underpredicted by the model by about 20%.

The wave impact theory model by Larson et al. (2004a) calculates recession distance and eroded volume, in time, for coastal dunes during severe storms. Wave impact theory assumes a linear relationship between the swash impact due to the change of momentum of the bores impacting the dune, F, and the weight of the sediment eroded from the dune face, ΔW. The dune toe retreats along the slope of the foreshore, β_f, and retreats up to a point until the eroded volume equals ΔW (Fig. 13). The swash force is computed using the velocity of the bore which can be related to the runup height. The model restricts itself to 1 single cell in which only the dune face and foreshore are included. It does not regard the coastal profile further seaward of the foreshore.

The model of Larson et al. (2004a) requires the storm conditions, the water level at the beginning of the swash zone, the foreslope of the coastal profile, the initial location of the dune toe, and a (empirical) transport coefficient as input parameters. To acquire the results of Fig. 13, the initial dune toe was set at a vertical elevation of 2.5 m. The foreshore slope was based on a linear fit of the bed profile 150 m in front of this dune toe. The vertical level of the beginning of the swash zone was defined as the surge level plus the wave setup, in which the setup was computed using the empirical expression of Stockdon et al. (2006). The applied storm conditions were equal to that of Fig. 12b. The transport coefficient, c_s, was set at $1.7 * 10^{-4}$. This value is advised by Larson et al. (2004a) for these specific wave conditions, and is based on the best fit in Larson et al. (2004a) for the dataset of Birkemeier et al. (1988).

The model of Larson et al. (2004a) was designed as a preliminary simplified analytical tool. Its physical basis is wave impact theory, but several empirical expressions are included to keep the model simple. No mention is made about the inclusion of non-erodible layers. Moreover, the solutions presented in Larson et al. (2004a) are further simplified by assuming no large vertical variation of the dune toe with time, because else the analytical solution becomes too complex. No mention is made about where the eroded sediment settles and the bathymetry changes in the sub-tidal area. This implies that the negative feedback mechanism that occurs during dune erosion is not incorporated in the model.

The cross-shore numerical model CSHORE, originally developed by Kobayashi et al. (2009), is described and reviewed in Kobayashi (2016). CSHORE is a model which, at the time of writing the review, assumes alongshore uniformity and cohesionless sediment, being sand, gravel or stone. Model hydrodynamics are depth averaged and based on a combined wave and current model, which uses the time-averaged continuity, cross-shore and alongshore momentum, wave action and roller energy equations. Sediment transport is divided into suspended and bed load transport, with empirically calibrated transport formulas.

CSHORE allows inclusion of permeable layers in the wet zone to account for permeability effects for gravel and stone beaches. Irregular runup and wet probability in the swash zone can be predicted using a probability function based on the time-averaged hydrodynamics, and these computations can be used to predict sediment transport there.

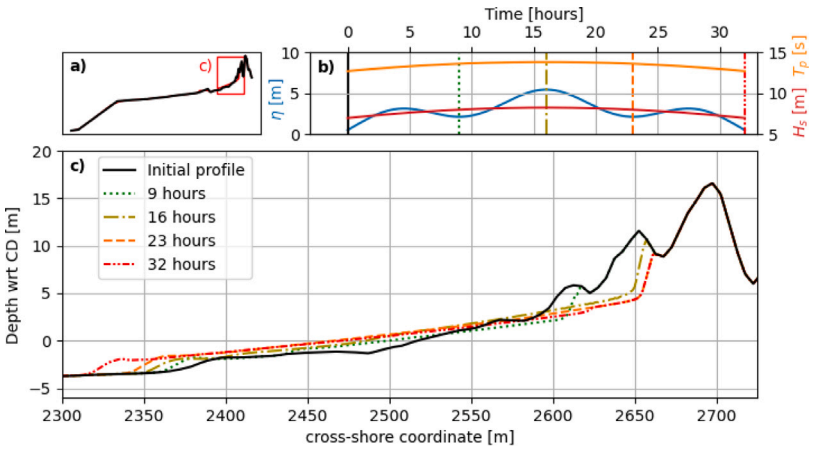

Fig. 12. Results of the DurosTA model of Steetzel (1993) with standard settings on the Meijendel transect. The storm conditions vary in time as displayed in (b), and the coloured profiles in (c) correspond to the moments in time displayed with vertical lines in (b). The total storm duration is 32 h.

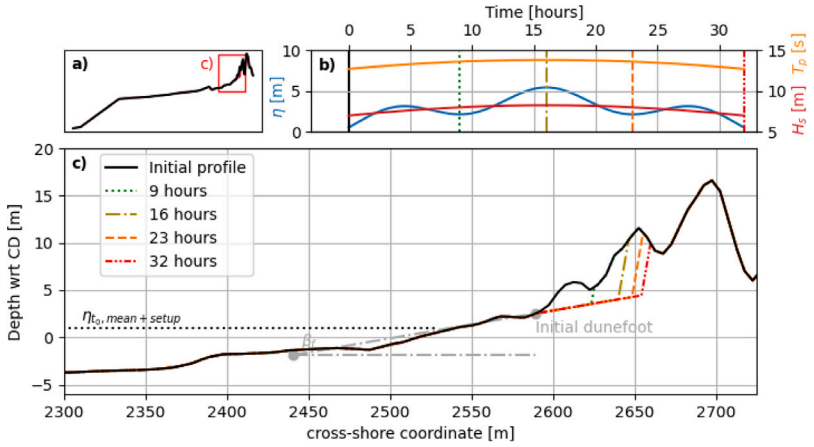

Fig. 13. Results of the wave impact model presented in Larson et al. (2004a) (c) on the Meijendel transect (a). The storm hydrograph is displayed in (b).

Kobayashi (2016) also addresses the interactions of waves with objects such as piles.

All models mentioned up to now are primarily cross-shore models which work with a 1-dimensional grid, or assume alongshore uniformity. DurosTA (Steetzel, 1991) works with a 1-dimensional grid, but does allow inclusion of alongshore processes such as alongshore currents generated by wave breaking. Morphologic change only occurs if there is an alongshore gradient of these flow velocities, which can for instance be the case for curved coastlines. Steetzel (1991) assumes these alongshore currents do not induce extra bed shearing, they purely act as a transport medium.

XBeach is an open-source process-based model which can operate in 1 or 2 dimensions (2DH) and solves equations for wave propagation, flow, sediment transport and bed level change (Roelvink et al., 2009). It can be run in stationary, surf beat, and nonhydrostatic mode. Surf beat mode facilitates relatively fast computations of dune response to storms and will be discussed here. In this mode short-wave energy is averaged and the wave forcing varies on the time-scale of wave groups. Using the wave action balance, the dissipation of wave energy is computed, which serves as a source for the roller energy balance. Both wave and roller energy are used to compute radiation stresses, and the gradients of these stresses are used to compute the flow field in the nearshore. Sediment transport is modelled with a depth-averaged advection diffusion equation after Galappatti and Vreugdenhil (1985). Spatial differences in sediment transport rates lead to accretion or sedimentation and subsequently bed level change in time. An avalanching mechanism is incorporated in the model through critical wet and dry slopes of the sediment. When the slope between 2 consecutive cells exceeds the critical value, sediment is redistributed to neighbouring cells until a slope equal to or smaller than the critical value is regained. 1D Model results are displayed in Fig. 14. In the 1D model, the waves are normally incident with a directional spreading of 30°, and based on a standard JONSWAP wave spectrum with wave parameters as displayed in Fig. 14b. Sediment properties are defined using a D_{50} instead of a sediment fall velocity. This D_{50} is used to compute the sediment fall velocity using the equation of Ahrens (2000). To acquire the results of Fig. 14, a D_{50} of 234 μm is used, which results in a fall velocity of 0.0268 m/s, consistent with the runs of the other models.

XBeach allows non-erodible layers and different sediment layers to be incorporated in the model. Also, dune vegetation can be modelled which will influence nearshore hydrodynamics. In addition, XBeach can be run in 2 dimensions (2DH), and therefore model 2-dimensional wave hydrodynamics and currents patterns accordingly. This is useful when the incident wave field is 2-dimensional with for instance oblique and directionally spread waves, or if there is significant alongshore variability or discontinuity of the coastline, near for instance harbour jetties, breakwaters, and strongly curved coastlines around headlands and bays. Fig. 15 presents results of a 2D model simulation of the coastal stretch around the 1D transect of Meijendel used earlier. The coastal stretch runs from 750 m below to 750 m above the central cross section of Figs. 11–14. The waves are obliquely incident with a main direction of 240°N, and a directional spreading of 30°, and are modelled as a standard JONSWAP wave spectrum with wave parameters as displayed in Fig. 14b.

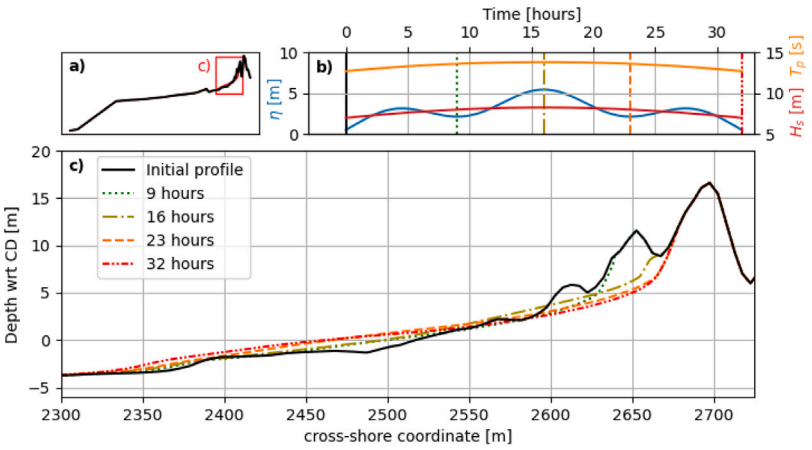

Fig. 14. XBeach 1D results for a run on the Meijendel transect. The storm conditions vary in time as displayed in (b). Waves are normally incident with a directional spreading of 30°.

The contours in Fig. 15 display that the coastal profile is 'reset' (after e.g. Price and Ruessink (2011)), in which complex 3D variabilities are smoothened out and depth contours become more shore parallel. The depth contours near the new dune toe (at approximately +6 m CD) are dense, and seaward they become sparse, implying a gentle beach profile with a steep dune scarp. The erosion and sedimentation patterns show that the troughs at x = 2400 m and 2600 m are infilled by sediment and smoothened out. The erosion at x = 2200 m indicates erosion of the offshore bar. The net erosion volumes of all cross sections are not completely uniform in alongshore direction, meaning that sediment is exchanged between cross sections. This indicates the importance of including alongshore variability in the coastal profile, because sediment is not necessarily conserved in a single cross section. This also exemplifies the possibility of having erosion hotspots along a coastal stretch in the model domain (Cohn et al., 2021).

4.3. Comparisons between models

4.3.1. Model sensitivities

The aforementioned models have multiple and sometimes different input parameters. In this section, the sensitivity of each model to the storm surge level (SSL), wave height (H_s), wave period (T_p), and sediment fall velocity (w_s) will be compared. Each parameter will be altered between 70% and 130% of its original value. For the sensitivity of XBeach to w_s, a D_{50} was picked that resulted in a w_s which was either 70, 85, 115, or 130% of the standard fall velocity according to Ahrens (2000). The sensitivity of Larson et al. to w_s is not computed, because its dependency is incorporated in the transport coefficient, c_s, but for the hydrodynamic conditions used in this comparison a standard value of $1.7 * 10^{-4}$ is advised by Larson et al. (2004a). Results of the comparison are displayed in Fig. 16.

All models show a strong dependency on the storm surge level (SSL): the difference between the 130 and 70% values of the SSL is greatest for all parameters, for all models. The model of van Gent et al. (2008) displays a stronger dependency on the wave height than the wave period, and reacts strongly to differences in sediment fall velocity. Overall, the van Gent et al. model shows the greatest variation for all parameters, which might be due to the fact that the imposed hydrodynamic conditions differ considerably from the reference values of the flume experiments on which the model is based. DurosTA (Steetzel, 1993) shows little reaction to changing wave heights. The dependency of DurosTA on the wave period is stronger, and of similar size as that of the sediment fall velocity. Larson et al.'s model reacts stronger on wave height alterations than wave period alterations. Last, XBeach 1D

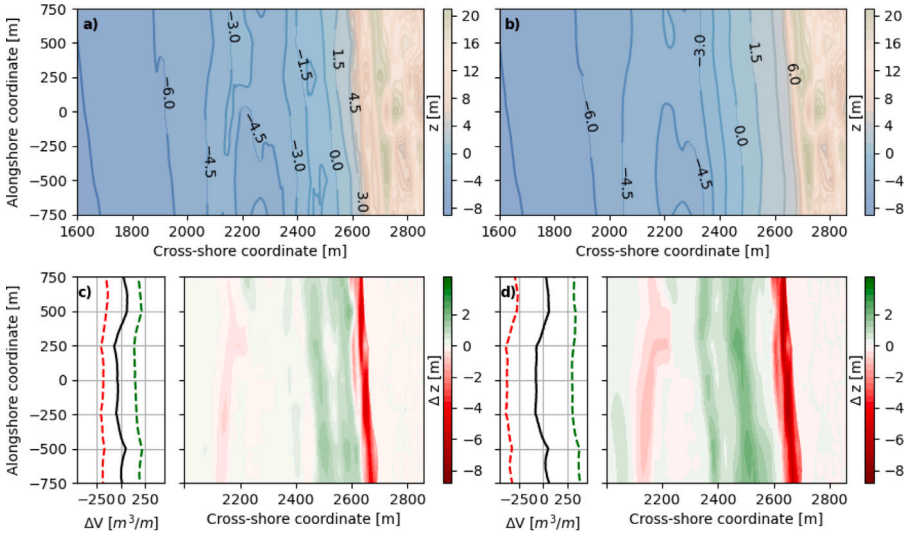

Fig. 15. XBeach 2D results for a run on the coastal stretch 750 m below and above the Meijendel transect (Fig. 14). The storm conditions vary in time for 32 h as displayed in Fig. 14(b). The waves are obliquely incident with a main direction of 240°N, and a directional spreading of 30°. Panels (a) and (b) display the contours of the initial bathymetry and final bathymetry respectively. Panels (c) and (d) display the erosion and sedimentation patters after 16 h and 32 h respectively. On the left of both panels, the total eroded (red), settled (green), an net (black) volumes in each cross section are shown.

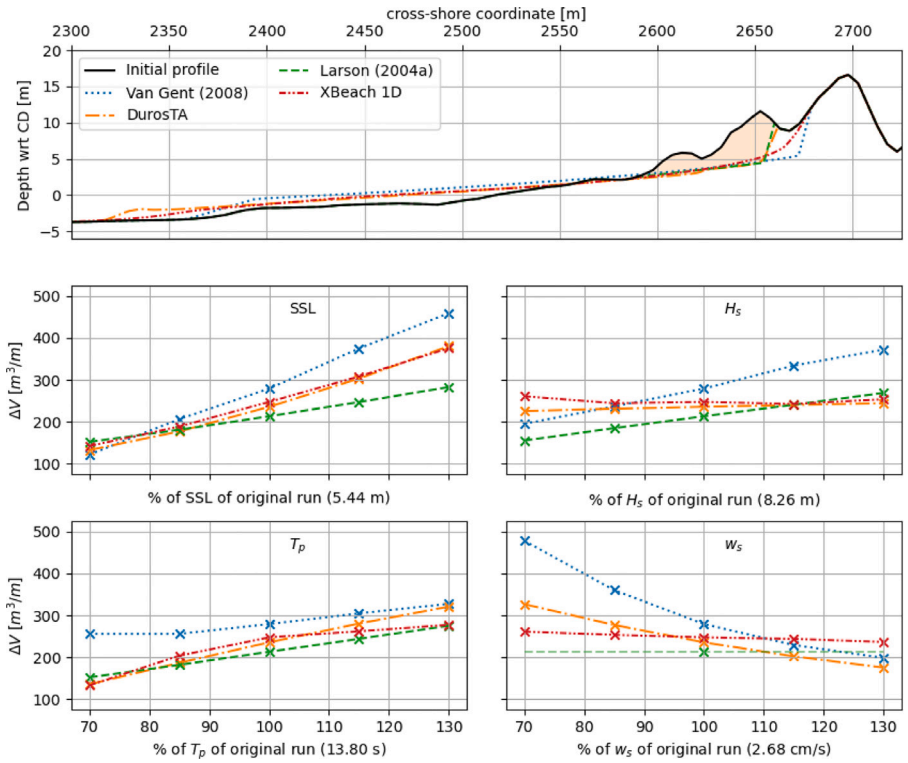

Fig. 16. Model sensitivities to SSL, H_s, T_p, and w_s. The upper panel displays the final profile of each model for the Meijendel transect when run with the standard hydrodynamic conditions. The lower panels display the eroded volume ΔV in [m^3/m], shoreward of x = 2300 m. The total eroded volume of DurosTA is displayed in yellow in the upper panel.

is second most sensitive to T_p, but shows little dependency on w_s and H_s. Interestingly enough, XBeach 1D actually predicts a larger eroded volume for the smallest wave height, which is due to more erosion at the lower base of the dune. The retreat of the dune crest remains largest for the largest wave height. Nevertheless, the differences are relatively small for a changing wave height.

Sensitivities to 2-dimensional effects such as wave obliquity can be analysed using DurosTA and XBeach 2D. Den Heijer (2013) found that DurosTA predicts decreasing erosion volumes with increasing wave angle with respect to the shore normal, while XBeach predicts increasing erosion volumes with increasing wave angle. One of the major reasons for this difference is that DurosTA uses the breaking induced turbulence to compute sediment concentrations, which results in smaller concentrations for oblique waves. XBeach includes bed shearing in the computation of sediment concentrations, and due to the generated alongshore currents, this results in larger concentrations for oblique waves up to approximately 40°. How wave directionality influences dune erosion from a physical perspective is something which, up to now, is not yet fully understood. Further research and field validation into wave obliquity is therefore recommended. The effect of directional spreading can be analysed with XBeach 2D. The model predicts less erosion for increasing spread, as less wave-wave interactions occur, reducing the transfer of energy to the lower frequencies and thereby decreasing the runup due to infragravity waves (Roelvink et al., 2018, after Herbers et al. (1994)).

4.3.2. Comparison of model predictions with the LIP11D experiments

The discussed equilibrium and process-based models can be validated using test 2E of the LIP11D experiments after Arcilla et al. (1994) (Fig. 17). It should be noted that this run is also used for the validation of XBeach in Roelvink et al. (2009). In run 2E, a dune was exposed for 18 h to a surge level of 4.6 m with waves with a significant height of 1.4 m and peak period of 5 s. The fall velocity of sediment samples taken during the experiment was analysed in the Delft Hydraulics Laboratory using a Visual Accumulation Tube (VAT). This fall velocity was converted to a D_{50} using formulae of Van Rijn (1989), which resulted in a D_{50} of 200 μm for test 2E. In the validation in this review, the D_{50} of 200 μm was converted back to the fall velocity w_s using Van Rijn (1989), which is 0.0257 m/s. To be consistent with earlier computations in this review, a new D_{50} is computed using the formula of Ahrens (2000) for the w_s of 0.0257 m/s. This resulted in a D_{50} of 227 μm, which will be used in the models in this comparison.

To acquire the results of Fig. 17, the models DUROS+ (van Gent et al., 2008) and DurosTA (Steetzel, 1993) were run in default mode. For the model of Larson et al. (2004a), the initial dune toe was defined as the sharp transition between the foreslope and dune face at x ≈ 183 m (black dot in Fig. 9). The foreslope, which is used as the slope with which the dune toe retreats, was based on the best linear fit through the dune toes in Fig. 9. Last, the angle of the dune face is set at 61.12° (after Fig. 9). For XBeach, first order wave steering was applied, because the flume tests were also performed with first-order wave generation. The critical dry slope was set on 1.813 (≈ tan(61.12°)). The profile was extended in offshore direction to a depth of 30 m in order to properly generate waves at the wavemaker boundary. No directional spreading was imposed on the waves.

Despite some deviations, all models are capable of predicting the post-storm profile reasonably well. The model of van Gent et al. (2008) seems to underpredict the amount of erosion and retreat of the dune crest. The model of Larson et al. (2004a) slightly underpredicts the amount of erosion, and XBeach slightly overpredicts it. DurosTA seems to accurately predict the post-storm profile for the given hydrodynamics and bathymetry. Fig. 18 shows the root mean squared error (RMSE) for the lower and upper part of the profile for all models, and is an indication of how accurate the shape of the bed profile is replicated by the models. The errors of the Larson et al. model and DurosTA seem to decrease with time for the upper part of the profile.

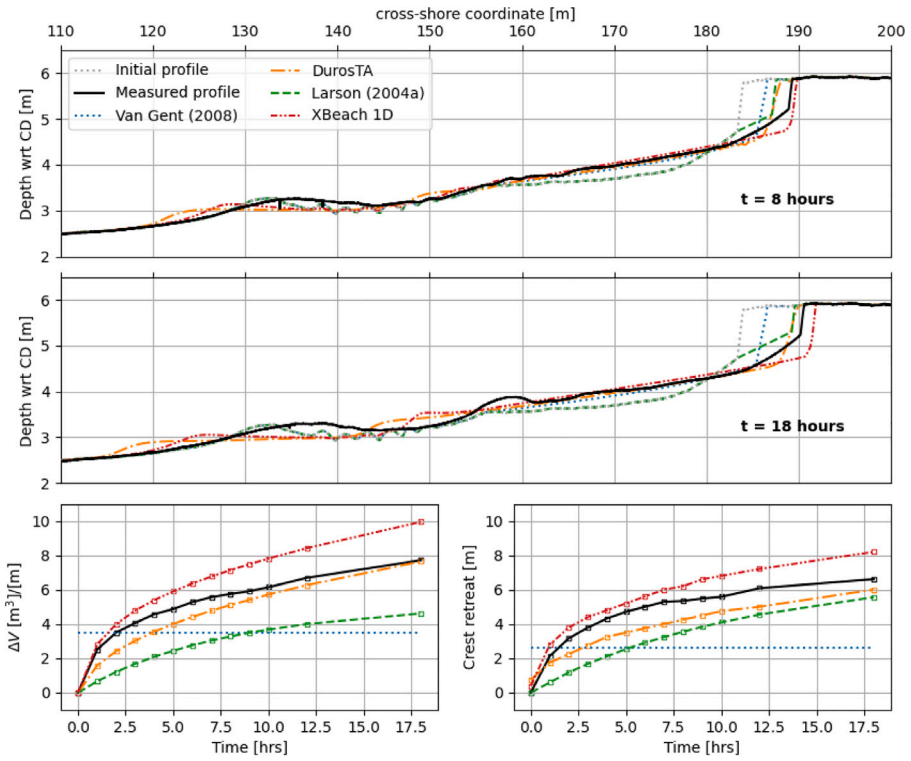

Fig. 17. Model predictions compared to the measured profile and volume changes for test 2E of the LIP11D experiments. The upper panel shows the measured and computed profiles after 8 h, the middle panel after 18 h. The lower two panels show the eroded volume of the dune (left) and the retreat of the dune crest (right) in time.

In summary, multiple dune erosion models have been developed over time, with differences in underlying physical processes and assumptions, complexities, and computational effort. With increasing knowledge on relevant hydrodynamic and morphodynamic processes comes the possibility of incorporating more of these processes in our modelling techniques, allowing for a broader range of coasts with different complexities to be analysed. However, as Figs. 17 and 18 point out, predictions differ between different models and there is no single model that results in accurate predictions for all cases. For some specific wave conditions and coastlines, an 'older' and simpler model, requiring less input parameters and computational effort, might prove the better tool. Nevertheless, once all the necessary input parameters are properly defined and calibrated, very accurate results can be acquired with process-based models (e.g. Roelvink et al. (2009), Bolle et al. (2011) and Schweiger et al. (2020)).

5. Conclusions

During dune erosion in the collision regime, the damage done to dunes can be significant with devastating floods as a potential consequence. By being able to understand and describe relevant physical processes, one can perform a proper risk assessment and take necessary coastal safety precautions. Over the past decades, field and laboratory observations have given more and new insights in relevant physical processes that occur during dune erosion. But despite these new insights, uncertainties and unknowns remain, especially around the effect of wave obliquity and the influence of dune vegetation on erosion rates. Moreover, sandy coastlines remain complex and may become more complex due to the presence of hard structures and multiple sediment layers. This reveals the many challenges that still remain.

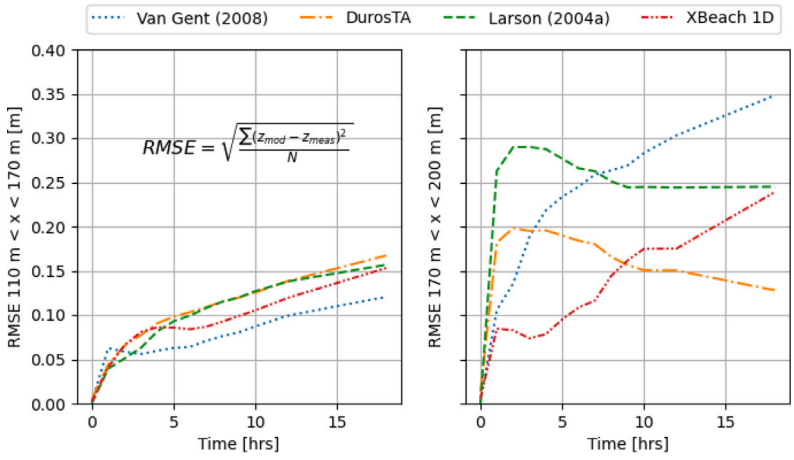

Fig. 18. RMSE for the modelled profiles with respect to the measured profiles for the lower segment, 110 m < x < 170 m (left) and the upper segment, 170 m < x < 200 m (right).

Many of the unknown processes regarding dune erosion prove difficult to investigate in a laboratory, which is often confined to a one-dimensional wave flume. On the other hand, field observations remain difficult due to the unpredictability of storms and the dangers storm conditions pose for observers. The concept of 'manipulative' field experiments might prove a solution to these issues. The new insights we might gain from such experiments could help us make more complete our modelling techniques. However, a more complete and complex model does not necessarily result in more accurate predictions. For specific wave conditions and coastlines, a computationally cheaper model such as an equilibrium model can already yield satisfactory results. Nevertheless, with continuously changing coastlines and intensifying storm conditions due to for instance sea level rise, further development of existing models and the creation of new models remains crucial for managing coastal resilience, and is therefore needed. Accurate and realistic modelling techniques allow identification of sandy coastlines where more safety precautions are necessary, but also areas where coastal protection is already overly conservative, which may leave room for the reintroduction of natural dynamics in dune landscapes.

Acknowledgements

This research was funded by Delft University of Technology, TKI Deltatechnology (Topconsortia for Knowledge and Innovation), Rijkswaterstaat (the Dutch Ministry of Infrastructure and Water Management), STOWA (the Dutch Waterboards), Deltares, Arcadis, and Witteveen+Bos.

Declaration of competing interest

The authors declare that they have no known competing financial interests or personal relationships that could have appeared to influence the work reported in this paper.

Data availability

The authors do not have permission to share data.

References

Aagaard, T., Greenwood, B., 2008. Infragravity wave contribution to surf zone sediment transport - the role of advection. Mar. Geol. 251 (1–2), 1–14. http://dx.doi.org/10.1016/j.margeo.2008.01.017.

Ahrens, J.P., 2000. A fall-velocity equation. J. Waterw. Port Coast. Ocean Eng. 126 (2), 99–102. http://dx.doi.org/10.1061/(asce)0733-950x(2000)126:2(99).

Arcilla, A., Roelvink, J., O'Connor, B., Reniers, A., Jimenez, J., 1994. The Delta flume '93 experiment. Coast. Dyn. 488–502.

Baart, F., Bakker, M.A., Van Dongeren, A., Den Heijer, C., Van Heteren, S., Smit, M.W., Van Koningsveld, M., Pool, A., 2011. Using 18th century storm-surge data from the Dutch Coast to improve the confidence in flood-risk estimates. Nat. Hazards Earth Syst. Sci. 11 (10), 2791–2801. http://dx.doi.org/10.5194/nhess-11-2791-2011.

Barbier, E.B., Koch, E.W., Silliman, B.R., Hacker, S.D., Wolanski, E., Primavera, J., Granek, E.F., Polasky, S., Aswani, S., Cramer, L.A., Stoms, D.M., Kennedy, C.J., Bael, D., Kappel, C.V., Perillo, G.M., Reed, D.J., 2008. Coastal ecosystem-based management with nonlinear ecological functions and values. Science 319 (5861), 321–323. http://dx.doi.org/10.1126/science.1150349.

Bertin, X., de Bakker, A., van Dongeren, A., Coco, G., André, G., Ardhuin, F., Bonneton, P., Bouchette, F., Castelle, B., Crawford, W.C., Davidson, M., Deen, M., Dodet, G., Guérin, T., Inch, K., Leckler, F., McCall, R., Muller, H., Olabarrieta, M., Roelvink, D., Ruessink, G., Sous, D., Stutzmann, E., Tissier, M., 2018. Infragravity waves: From driving mechanisms to impacts. Earth-Sci. Rev. 177, 774–799. http://dx.doi.org/10.1016/j.earscirev.2018.01.002.

Birkemeier, W.A., Savage, R.J., Leffler, M.W., 1988. A Collection of Storm Erosion Field Data. Technical Report CERC-88-9, US Department of the Army, Corps of Engineers.

Bolle, A., Mercelis, P., Roelvink, D., Haerens, P., Trouw, K., 2011. Application and validation of xbeach for three different field sites. Coast. Eng. Proc. 1 (32), 40. http://dx.doi.org/10.9753/icce.v32.sediment.40.

Bonte, Y., Levoy, F., 2015. Field experiments of beach scarp erosion during oblique wave, stormy conditions (normandy, France). Geomorphology 236, 132–147. http://dx.doi.org/10.1016/j.geomorph.2015.02.014.

Bowen, A.J., 1969. The generation of longshore currents on a plane beach. J. Mar. Res. 27 (2), 206–215.

Bowen, A., Doering, J., 1984. Nearshore sediment transport: estimates from detailed measurements of the nearshore velocity field. Coast. Eng. Proc. 1 (19), 115. http://dx.doi.org/10.9753/icce.v19.115.

Bruun, P., 1954. Coast Erosion and the Development of Beach Profiles, forty-fourth ed. US Beach Erosion Board.

Butt, T., Russell, P., 1999. Suspended sediment transport mechanisms in high-energy swash. Mar. Geol. 161 (2–4), 361–375. http://dx.doi.org/10.1016/S0025-3227(99)00043-2.

Butt, T., Russell, P., Puleo, J., Miles, J., Masselink, G., 2004. The influence of bore turbulence on sediment transport in the swash and inner surf zones. Cont. Shelf Res. 24 (7–8), 757–771. http://dx.doi.org/10.1016/j.csr.2004.02.002.

Castelle, B., Marieu, V., Bujan, S., Splinter, K.D., Robinet, A., Sénéchal, N., Ferreira, S., 2015. Impact of the winter 2013–2014 series of severe western europe storms on a double-barred sandy coast: Beach and dune erosion and megacusp embayments. Geomorphology 238, 135–148. http://dx.doi.org/10.1016/J.GEOMORPH.2015.03.006.

Cohn, N., Brodie, K.L., Johnson, B., Palmsten, M.L., 2021. Hotspot dune erosion on an intermediate beach. Coast. Eng. 170, 103998. http://dx.doi.org/10.1016/j.coastaleng.2021.103998.

Cohn, N., Ruggiero, P., García-Medina, G., Anderson, D., Serafin, K.A., Biel, R., 2019. Environmental and morphologic controls on wave-induced dune response. Geomorphology 329, 108–128. http://dx.doi.org/10.1016/j.geomorph.2018.12.023.

Dally, W.R., Dean, R.G., 1984. Suspended sediment transport and beach profile evolution. J. Waterw. Port Coast. Ocean Eng. 110 (1), 15–33. http://dx.doi.org/10.1061/(ASCE)0733-950X(1984)110:1(15).

Davidson, S.G., Hesp, P.A., da Silva, G.M., 2020. Controls on dune scarping. Progress in Physical Geography: Earth and Environment 44 (6), 923–947. http://dx.doi.org/10.1177/0309133320932880.

de Winter, R.C., Gongriep, F., Ruessink, B.G., 2015. Observations and modeling of alongshore variability in dune erosion at egmond aan zee, the netherlands. Coast. Eng. 99, 167–175. http://dx.doi.org/10.1016/j.coastaleng.2015.02.005.

Dean, R.G., 1977. Equilibrium Beach Profiles: US Atlantic and Gulf Coasts. Department of Civil Engineering and College of Marine Studies, University of Florida.

Den Heijer, C., 2013. The Role of Bathymetry, Wave Obliquity and Coastal Curvature in Dune Erosion Prediction (Ph.D. thesis). Delft University of Technology, pp. 1–173.

Dyhr-Nielsen, M., Sørensen, T., 1970. Some sand transport phenomena on coasts with bars. In: Coastal Engineering 1970. American Society of Civil Engineers, New York, NY, pp. 855–865. http://dx.doi.org/10.1061/9780872620285.054.

Edelman, T., 1972. Dune erosion during storm conditions. In: Proc. 13Th Coastal Engng. Conf. (Vancouver), Vol. 2. pp. 1305–1311. http://dx.doi.org/10.1061/9780872620490.073.

Erikson, L.H., Larson, M., Hanson, H., 2007. Laboratory investigation of beach scarp and dune recession due to notching and subsequent failure. Mar. Geol. 245 (1–4), 1–19. http://dx.doi.org/10.1016/j.margeo.2007.04.006.

Feagin, R.A., Furman, M., Salgado, K., Martinez, M.L., Innocenti, R.A., Eubanks, K., Figlus, J., Huff, T.P., Sigren, J., Silva, R., 2019. The role of beach and sand dune vegetation in mediating wave run up erosion. Estuar. Coast. Shelf Sci. 219, 97–106. http://dx.doi.org/10.1016/j.ecss.2019.01.018.

Fiedler, J.W., Brodie, K.L., McNinch, J.E., Guza, R.T., 2015. Observations of runup and energy flux on a low-slope beach with high-energy, long-period ocean swell. Geophys. Res. Lett. 42 (22), 9933–9941. http://dx.doi.org/10.1002/2015GL066124.

Figlus, J., Sigren, J.M., Armitage, A.R., Tyler, R.C., 2014. Erosion of Vegetated Coastal dunes. Coast. Eng. Proc. 1 (34), 20. http://dx.doi.org/10.9753/icce.v34.sediment.20.

Figlus, J., Sigren, J.M., Feagin, R.A., Armitage, A.R., 2022. The unique ability of fine roots to reduce Vegetated Coastal dune erosion during wave collision. Front. Built Environ. 8, 129. http://dx.doi.org/10.3389/fbuil.2022.904837.

Fisher, J.S., Overton, M.F., 1985. Numerical model for dune erosion due to wave uprush. In: Proceedings of the Coastal Engineering Conference, Vol. 2. pp. 1553–1558. http://dx.doi.org/10.1061/9780872624382.106.

Fisher, J.S., Overton, M.F., Chisholm, T., 1986. Field measurements of dune erosion. Coast. Eng. 2 (11), 1107–1115. http://dx.doi.org/10.1061/9780872626003.082.

Galappatti, G., Vreugdenhil, C.B., 1985. A depth-integrated model for suspended sediment transport. J. Hydraul. Res. 23 (4), 359–377. http://dx.doi.org/10.1080/00221688509499345.

Gallagher, E.L., Elgar, S., Guza, R.T., 1998. Observations of sand bar evolution on a natural beach. J. Geophys. Res.: Oceans 103 (C2), 3203–3215. http://dx.doi.org/10.1029/97jc02765.

Guza, R.T., Thornton, E.B., 1982. Swash oscillations on a natural beach. J. Geophys. Res. 87 (C1), 483–491. http://dx.doi.org/10.1029/JC087iC01p00483.

Harley, M.D., Turner, I.L., Splinter, K.D., Phillips, M.S., Simmons, J.A., 2016. Beach response to Australian east coast lows: A comparison between the 2007 and 2015 events, narrabeen-collaroy beach. J. Coast. Res. 1 (75), 388–392. http://dx.doi.org/10.2112/SI75-078.1.

Hasselmann, K., 1962. On the non-linear energy transfer in a gravity-wave spectrum: Part 1. general theory. J. Fluid Mech. 12 (4), 481–500. http://dx.doi.org/10.1017/S0022112062000373.

Herbers, T.H.C., Elgar, S., Guza, R.T., 1994. Infragravity-frequency (0.005–0.05 hz) motions on the shelf. Part I: Forced waves. J. Phys. Oceanogr. 24 (5), 917–927. http://dx.doi.org/10.1175/1520-0485(1994)024<0917:IFHMOT>2.0.CO;2.

Herbers, T.H., Elgar, S., Guza, R.T., 1995. Generation and propagation of infragravity waves. J. Geophys. Res. 100 (C12), http://dx.doi.org/10.1029/95jc02680.

Hughes, S.A., 1981. Beach and Dune Erosion During Severe Storms (Ph.D. thesis). University of Florida, Florida.

Hughes, M.G., Aagaard, T., Baldock, T.E., Power, H.E., 2014. Spectral signatures for swash on reflective, intermediate and dissipative beaches. Mar. Geol. 355, 88–97. http://dx.doi.org/10.1016/j.margeo.2014.05.015.

Itzkin, M., Moore, L.J., Ruggiero, P., Hacker, S.D., Biel, R.G., 2021. The relative influence of dune aspect ratio and beach width on dune erosion as a function of storm duration and surge level. Earth Surface Dynamics 9 (5), 1223–1237. http://dx.doi.org/10.5194/esurf-9-1223-2021.

Kobayashi, N., 1987. Analytical solution for dune erosion by storms. J. Waterw. Port Coast. Ocean Eng. 113 (4), 401–418. http://dx.doi.org/10.1061/(asce)0733-950x(1987)113:4(401).

Kobayashi, N., 2016. Coastal sediment transport modeling for engineering applications. J. Waterw. Port Coast. Ocean Eng. 142 (6), 03116001. http://dx.doi.org/10.1061/(asce)ww.1943-5460.0000347.

Kobayashi, N., Buck, M., Payo, A., Johnson, B.D., 2009. Berm and dune erosion during a storm. J. Waterw. Port Coast. Ocean Eng. 135 (1), 1–10. http://dx.doi.org/10.1061/(asce)0733-950x(2009)135:1(1).

Kobayashi, N., Gralher, C., Do, K., 2013. Effects of woody plants on dune erosion and overwash. J. Waterw. Port Coast. Ocean Eng. 139 (6), 466–472. http://dx.doi.org/10.1061/(asce)ww.1943-5460.0000200.

Kriebel, D.L., Dean, R.G., 1985. Numerical simulation of time-dependent beach and dune erosion. Coast. Eng. 9 (3), 221–245. http://dx.doi.org/10.1016/0378-3839(85)90009-2.

Larson, M., Erikson, L., Hanson, H., 2004a. An analytical model to predict dune erosion due to wave impact. Coast. Eng. 51 (8–9), 675–696. http://dx.doi.org/10.1016/j.coastaleng.2004.07.003.

Larson, M., Kraus, N.C., 1989. SBEACH: Numerical Model for Simulating Storm-Induced Beach Change; Report 1: Empirical Foundation and Model Development. Technical Report, US Army Coastal Engineering Research Center.

Larson, M., Kubota, S., Erikson, L., 2004b. Swash-zone sediment transport and foreshore evolution: field experiments and mathematical modeling. Mar. Geol. 212 (1–4), 61–79. http://dx.doi.org/10.1016/j.margeo.2004.08.004.

Lippmann, T.C., Holman, R.A., 1990. The spatial and temporal variability of sand bar morphology. J. Geophys. Res. 95 (C7), http://dx.doi.org/10.1029/jc095ic07p11575.

Longuet-Higgins, M.S., 1970. Longshore currents generated by obliquely incident sea waves- 1, 2. J. Geophys. Res. 75 (33), 6778–6801. http://dx.doi.org/10.1029/jc075i033p06790.

Longuet-Higgins, M.S., Stewart, R.W., 1962. Radiation stress and mass transport in gravity waves, with application to 'surf beats'. J. Fluid Mech. 13 (4), 481–504. http://dx.doi.org/10.1017/S0022112062000877.

Longuet-Higgins, M.S., Stewart, R.w., 1964. Radiation stresses in water waves; a physical discussion, with applications. Deep-Sea Res. Oceanogr. Abstr. 11 (4), 529–562. http://dx.doi.org/10.1016/0011-7471(64)90001-4.

Madsen, O.S., 1975. Stability of a sand bed under breaking waves. In: Coastal Engineering Proceedings, Vol. 14. ASCE, pp. 776–794. http://dx.doi.org/10.9753/icce.v14.45.

Masselink, G., Castelle, B., Scott, T., Dodet, G., Suanez, S., Jackson, D., Floc'H, F., 2016a. Extreme wave activity during 2013/2014 winter and morphological impacts along the atlantic coast of europe. Geophys. Res. Lett. 43 (5), 2135–2143. http://dx.doi.org/10.1002/2015GL067492.

Masselink, G., Evans, D., Hughes, M.G., Russell, P., 2005. Suspended sediment transport in the swash zone of a dissipative beach. Mar. Geol. 216 (3), 169–189. http://dx.doi.org/10.1016/j.margeo.2005.02.017.

Masselink, G., Puleo, J.A., 2006. Swash-zone morphodynamics. http://dx.doi.org/10.1016/j.csr.2006.01.015.

Masselink, G., Scott, T., Poate, T., Russell, P., Davidson, M., Conley, D., 2016b. The extreme 2013/2014 winter storms: Hydrodynamic forcing and coastal response along the southwest coast of England. Earth Surf. Process. Landf. 41 (3), 378–391. http://dx.doi.org/10.1002/esp.3836.

Mendoza, E., Odériz, I., Martínez, M.L., Silva, R., 2017. Measurements and modelling of small scale processes of vegetation preventing dune erosion. J. Coast. Res. 77, 19–27. http://dx.doi.org/10.2112/SI77-003.1.

Moller, J., Swart, D., 1988. Extreme erosion event on an artificial beach. Coast. Eng. 1882–1896.

Munk, W.H., 1950. Origin and generation of waves. Coast. Eng. Proc. 1 (1), 1. http://dx.doi.org/10.9753/ICCE.V1.1.

Nielsen, P., 1992. Coastal Bottom Boundary Layers and Sediment Transport, fourth ed. World scientific.

Nishi, R., Sato, M., Wang, H., 1994. Field observation and numerical simulation of beach and dune scarps. Coast. Eng. Proc. 1 (24), 2434–2448. http://dx.doi.org/10.1061/9780784400890.177.

Odériz, I., Knöchelmann, N., Silva, R., Feagin, R.A., Martínez, M.L., Mendoza, E., 2020. Reinforcement of vegetated and unvegetated dunes by a rocky core: A viable alternative for dissipating waves and providing protection? Coast. Eng. 158, 103675. http://dx.doi.org/10.1016/j.coastaleng.2020.103675.

Osborne, P.D., Greenwood, B., 1992. Frequency dependent cross-shore suspended sediment transport. 2. A barred shoreface. Mar. Geol. 106 (1–2), 25–51. http://dx.doi.org/10.1016/0025-3227(92)90053-K.

Osborne, P.D., Rooker, G.A., 1999. Sand re-suspension events in a high energy infragravity swash zone. J. Coast. Res. 15 (1), 74–86.

Overbeck, J.R., Long, J.W., Stockdon, H.F., 2017. Testing model parameters for wave-induced dune erosion using observations from hurricane sandy. Geophys. Res. Lett. 44 (2), 937–945. http://dx.doi.org/10.1002/2016GL071991.

Overton, M.F., Fisher, J.S., Young, M.A., 1988. Laboratory investigation of dune erosion. J. Waterw. Port Coast. Ocean Eng. 114 (3), 367–373. http://dx.doi.org/10.1061/(asce)0733-950x(1988)114:3(367).

Overton, M.F., Pratikto, W.A., Lu, J.C., Fisher, J.S., 1994. Laboratory investigation of dune erosion as a function of sand grain size and dune density. Coast. Eng. 23 (1–2), 151–165. http://dx.doi.org/10.1016/0378-3839(94)90020-5.

Palmsten, M.L., Holman, R.A., 2011. Infiltration and instability in dune erosion. J. Geophys. Res.: Oceans 116 (10), C10030. http://dx.doi.org/10.1029/2011JC007083.

Palmsten, M.L., Holman, R.A., 2012. Laboratory investigation of dune erosion using stereo video. Coast. Eng. 60 (1), 123–135. http://dx.doi.org/10.1016/j.coastaleng.2011.09.003.

Price, T.D., Ruessink, B.G., 2011. State dynamics of a double sandbar system. Cont. Shelf Res. 31 (6), 659–674. http://dx.doi.org/10.1016/j.csr.2010.12.018.

Puleo, J.A., Beach, R.A., Holman, R.A., Allen, J.S., 2000. Swash zone sediment suspension and transport and the importance of bore-generated turbulence. J. Geophys. Res.: Oceans 105 (C7), 17021–17044. http://dx.doi.org/10.1029/2000jc900024.

Ranasinghe, R., Symonds, G., Black, K., Holman, R., 2004. Morphodynamics of intermediate beaches: A video imaging and numerical modelling study. Coast. Eng. 51 (7), 629–655. http://dx.doi.org/10.1016/j.coastaleng.2004.07.018.

Raubenheimer, B., Guza, R.T., 1996. Observations and predictions of run-up. J. Geophys. Res. C 101 (C11), 25575–25587. http://dx.doi.org/10.1029/96JC02432.

Reniers, A.J., Roelvink, J.A., Thornton, E.B., 2004a. Morphodynamic modeling of an embayed beach under wave group forcing. J. Geophys. Res.: Oceans 109 (1), http://dx.doi.org/10.1029/2002jc001586.

Reniers, A.J., Thornton, E.B., Stanton, T.P., Roelvink, J.A., 2004b. Vertical flow structure during sandy duck: Observations and modeling. Coast. Eng. 51 (3), 237–260. http://dx.doi.org/10.1016/j.coastaleng.2004.02.001.

Roelvink, D., McCall, R., Mehvar, S., Nederhoff, K., Dastgheib, A., 2018. Improving predictions of swash dynamics in xbeach: The role of groupiness and incident-band runup. Coast. Eng. 134, 103–123. http://dx.doi.org/10.1016/j.coastaleng.2017.07.004.

Roelvink, D., Reniers, A., van Dongeren, A., van Thiel de Vries, J., McCall, R., Lescinski, J., 2009. Modelling storm impacts on beaches, dunes and barrier islands. Coast. Eng. 56 (11–12), 1133–1152. http://dx.doi.org/10.1016/j.coastaleng.2009.08.006.

Roelvink, J.A., Stive, M.F., 1989. Bar-generating cross-shore flow mechanisms on a beach. J. Geophys. Res. 94 (C4), 4785–4800. http://dx.doi.org/10.1029/JC094iC04p04785.

Ruessink, B.G., Houwman, K.T., Hoekstra, P., 1998. The systemic contribution of transporting mechanisms to the cross-shore sediment transport in water depths of 3 to 9 m. Mar. Geol. 152 (4), 295–324. http://dx.doi.org/10.1016/S0025-3227(98)00133-9.

Sallenger, J., 2000. Storm impact scale for barrier islands. J. Coast. Res. 16 (3), 890–895.

Schijf, J., 1972. Richtlijn Voor De Berekening Van Duinafslag Tengevolge Van Een Stormvloed. Technical Report, Technische Adviescommissie voor de Waterkeringen.

Schweiger, C., Kaehler, C., Koldrack, N., Schuettrumpf, H., 2020. Spatial and temporal evaluation of storm-induced erosion modelling based on a two-dimensional field case including an artificial unvegetated research dune. Coast. Eng. 161, http://dx.doi.org/10.1016/j.coastaleng.2020.103752.

Senechal, N., Abadie, S., Gallagher, E., MacMahan, J., Masselink, G., Michallet, H., Reniers, A., Ruessink, G., Russell, P., Sous, D., Turner, I., Ardhuin, F., Bonneton, P., Bujan, S., Capo, S., Certain, R., Pedreros, R., Garlan, T., 2011. The ECORS-truc vert'08 nearshore field experiment: Presentation of a three-dimensional morphologic system in a macro-tidal environment during consecutive extreme storm conditions. Ocean Dyn. 61 (12), 2073–2098. http://dx.doi.org/10.1007/s10236-011-0472-x.

Seymour, R., Guza, R.T., O'Reilly, W., Elgar, S., 2005. Rapid erosion of a small southern california beach fill. Coast. Eng. 52 (2), 151–158. http://dx.doi.org/10.1016/j.coastaleng.2004.10.003.

Silva, R., Martínez, M.L., Odériz, I., Mendoza, E., Feagin, R.A., 2016. Response of vegetated dune-beach systems to storm conditions. Coast. Eng. 109, 53–62. http://dx.doi.org/10.1016/j.coastaleng.2015.12.007.

Smith, G.G., Mocke, G.P., 2002. Interaction between breaking/broken waves and infragravity-scale phenomena to control sediment suspension transport in the surf zone. Mar. Geol. 187 (3–4), 329–345. http://dx.doi.org/10.1016/S0025-3227(02)00385-7.

Splinter, K.D., Palmsten, M.L., 2012. Modeling dune response to an East Coast low. Mar. Geol. 329–331, 46–57. http://dx.doi.org/10.1016/j.margeo.2012.09.005.

Steetzel, H.J., 1991. Cross-shore transport during storm surges. The dutch coast. Paper no. 6. In: Proceedings of the Coastal Engineering Conference, Vol. 2. American Society of Civil Engineers, New York, NY, pp. 1922–1934. http://dx.doi.org/10.1061/9780872627765.147.

Steetzel, H.J., 1992. Krokus-Stormen : Duinafslag Voorjaarsstormen 1990; Toetsing DUROSTA En Procedure Vaststelling Hydraulische Randvoorwaarden : Deel III Verslag Onderzoek. Technical Report, Rijkswaterstaat.

Steetzel, H.J., 1993. Cross-Shore Transport during Storm Surges (Ph.D. thesis). Delft University of Technology, http://dx.doi.org/10.1061/9780872627765.147.

Stive, M.J., Reniers, A.J., 2003. Sandbars in motion. Science 299 (5614), 1855–1856. http://dx.doi.org/10.1126/SCIENCE.1082512/ASSET/2043D011-BDD0-4DCB-A00B-3E92779B77EB/ASSETS/GRAPHIC/1855-1.GIF.

Stive, M.J., Wind, H.G., 1986. Cross-shore mean flow in the surf zone. Coast. Eng. 10 (4), 325–340. http://dx.doi.org/10.1016/0378-3839(86)90019-0.

Stockdon, H.F., Holman, R.A., Howd, P.A., Sallenger, A.H., 2006. Empirical parameterization of setup, swash, and runup. Coast. Eng. 53 (7), 573–588. http://dx.doi.org/10.1016/j.coastaleng.2005.12.005.

Thornton, E.B., Guza, R.T., 1986. Surf zone longshore currents and random waves: Field data and models. J. Phys. Oceanogr. 16 (7), 1165–1178. http://dx.doi.org/10.1175/1520-0485(1986)016<1165:SZLCAR>2.0.CO;2.

Thornton, E.B., Humiston, R.T., Birkemeier, W., 1996. Bar/trough generation on a natural beach. J. Geophys. Res. C 101 (C5), 12097–12110. http://dx.doi.org/10.1029/96JC00209.

Thornton, E.B., MacMahan, J., Sallenger, A.H., 2007. Rip currents, mega-cusps, and eroding dunes. Mar. Geol. 240 (1–4), 151–167. http://dx.doi.org/10.1016/J.MARGEO.2007.02.018.

van Bemmelen, C.W., de Schipper, M.A., Darnall, J., Aarninkhof, S.G., 2020. Beach scarp dynamics at nourished beaches. Coast. Eng. 160, 103725. http://dx.doi.org/10.1016/j.coastaleng.2020.103725.

van de Graaff, J., 1977. Dune erosion during a storm surge. Coast. Eng. 1 (C), 99–134. http://dx.doi.org/10.1016/0378-3839(77)90010-2.

van Dongeren, A., Battjes, J., Janssen, T., van Noorloos, J., Steenhauer, K., Steenbergen, G., Reniers, A., 2007. Shoaling and shoreline dissipation of low-frequency waves. J. Geophys. Res. 112 (C2), C02011. http://dx.doi.org/10.1029/2006JC003701.

van Gent, M.R., van Thiel de Vries, J.S., Coeveld, E.M., de Vroeg, J.H., van de Graaff, J., 2008. Large-scale dune erosion tests to study the influence of wave periods. Coast. Eng. 55 (12), 1041–1051. http://dx.doi.org/10.1016/j.coastaleng.2008.04.003.

van Houdt (Dutch Ministry of Infrastructure and Water Management), J., 2008. Photograph vlieland. URL: https://beeldbank.rws.nl.

van Rijn, L.C., 1984. Sediment transport, part III: Bed forms and alluvial roughness. J. Hydraul. Eng. 110 (12), 1733–1754. http://dx.doi.org/10.1061/(ASCE)0733-9429(1984)110:12(1733).

Van Rijn, L.C., 1989. Handbook Sediment Transport by Currents and Waves. Delft Hydraulics Report H461.

Van Thiel De Vries, J.S., Clarke, L.B., Aarninkhof, S.G., Coeveld, E.M., Holman, R.A., Palmsten, M.L., Reniers, A.J., Stive, M.J., Uijttewaal, W.S., 2007. Interaction of dune face and swash zone. In: Coastal Sediments '07 - Proceedings of 6th International Symposium on Coastal Engineering and Science of Coastal Sediment Processes. American Society of Civil Engineers, Reston, VA, pp. 1975–1987. http://dx.doi.org/10.1061/40926(239)155.

van Thiel de Vries, J., van Dongeren, A., McCall, R., Reniers, A., 2011. The effect of the longshore dimension on dune erosion. Coast. Eng. Proc. 1 (32), 49. http://dx.doi.org/10.9753/icce.v32.sediment.49.

van Thiel de Vries, J.S., van Gent, M.R., Walstra, D.J., Reniers, A.J., 2008. Analysis of dune erosion processes in large-scale flume experiments. Coast. Eng. 55 (12), 1028–1040. http://dx.doi.org/10.1016/j.coastaleng.2008.04.004.

Vellinga, P., 1978. Duinafslag Ten Gevolge Van De Stormvloed Op 3 Januari 1976; Toetsing Van De Voorlopige Richtlijn. Technical Report, Waterbouwkundig Laboratorium.

Vellinga, P., 1981. Schaalserie Duinafslag. Tekst en tabellen en Figuren. Verslag Modelonderzoek. M1263. Deel IIA. Technical Report, Delft Hydraulics.

Vellinga, P., 1982. Beach and dune erosion during storm surges. Coast. Eng. 6 (4), 361–387. http://dx.doi.org/10.1016/0378-3839(82)90007-2.

Vellinga, P., 1986. Beach and Dune Erosion during Storm Surges (Ph.D. thesis). Delft University of Technology.

Wright, L.D., Short, A.D., 1984. Morphodynamic variability of surf zones and beaches: A synthesis. Mar. Geol. 56 (1–4), 93–118. http://dx.doi.org/10.1016/0025-3227(84)90008-2.